https://doi.org/10.5194/egusphere-2026-6541
Preprint. Discussion started: 29 October 2026
© Author(s) 2026. CC BY 4.0 License.

The Anammox to Denitrification Ratio and its Environmental Controls in the Eastern Tropical Pacific

Jana Härri[1], Meike Vogt[1], and Nicolas Gruber[1]

[1]Environmental Physics, Institute of Biogeochemistry and Pollutant Dynamics, ETH Zurich, Zürich, Switzerland.

Correspondence: Jana Härri (jana.haerri@usys.ethz.ch)

Abstract. Water-column nitrogen (N) loss, driven by anammox and denitrification, accounts for ∼40% of global oceanic N loss, but the relative contribution of the two pathways remains unresolved. Stoichiometry predicts that, at steady state, anammox can account for at most 29% of N loss in anoxic waters, while observations from the Eastern Tropical Pacific (ETP) show that anammox frequently dominates N loss. Knowing the relative contribution of each pathway matters because only denitrification produces the potent greenhouse gas N_2O as an intermediate. Here, we couple the regional model ROMS-BEC with a nitrogen cycle module (NitrOMZ) to resolve the contribution of both pathways to N loss across the ETP. The model reproduces the high anammox to denitrification ratio observed at the sampling locations but yields a ratio of 32:68 when integrated over the entire water column of the ETP, close to the stoichiometrically expected ratio of 29:71. Hence, the apparent mismatch between the stoichiometrically expected and observed ratios in the ETP mainly arises from spatial and, to a lesser extent, temporal sampling biases. Short-lived denitrification pulses missed by discrete sampling, previously proposed to explain the low observed contribution of denitrification, account only partially for this mismatch. Overall, the anammox to denitrification ratio is mainly controlled by oxygen and increases with oxygen concentration. In addition, we find that high anammox to denitrification ratios locally coincide with net N_2O production and low ratios with net N_2O consumption, although this relationship breaks down at larger spatial and longer temporal scales. These findings advance our understanding of N loss and its implications for N_2O production and highlight undersampled regions that may be important to monitor as oxygen minimum zones change in extent and structure under global change.

1 Introduction

Fixed nitrogen (N) availability exerts a strong control on marine primary productivity, carbon export by the ocean's biological carbon pump, and thereby on the ocean's role in the global carbon cycle (Falkowski, 1997; Moore et al., 2013). Here, fixed N refers to all forms of biologically available N, except dinitrogen (N_2). The oceanic inventory of fixed N is maintained by a balance between N inputs from N_2 fixation, river input, and atmospheric deposition, and N losses through microbial processes in the water column and sediments, and through burial (Gruber, 2008; Wang et al., 2019). The Eastern Tropical Pacific (ETP) is a hotspot of N loss, with an estimated 39–70 Tg N y^{-1} of N loss occurring in its two oxygen minimum zones (OMZs, Deutsch et al., 2001; Bianchi et al., 2012; DeVries et al., 2013; Yang et al., 2017). In these low-oxygen environments, fixed N is converted to inert N_2 through two microbially mediated pathways: anaerobic ammonium oxidation (anammox) and classical

https://doi.org/10.5194/egusphere-2026-6541
Preprint. Discussion started: 29 October 2026
© Author(s) 2026. CC BY 4.0 License.

denitrification (Devol, 2008). Of these two pathways, only the multi-step denitrification process produces nitrous oxide (N_2O), a potent greenhouse gas, as an intermediate. With OMZs in the ETP projected to change in extent and structure (Busecke et al., 2022), and anthropogenic N deposition increasing (Fowler et al., 2013), understanding the balance between anammox and denitrification is critical for predicting future changes in marine N loss and the oceanic N_2O budget.

Anammox and denitrification partially compete for the same substrates but differ in their metabolic requirements and oxygen sensitivities. Anammox is a chemolithoautotrophic process that converts nitrite (NO_2^-) and ammonium (NH_4^+) to N_2 (Devol, 2008). Its activity depends on the local balance between processes that supply NH_4^+, such as the remineralization of organic matter, and those that supply NO_2^-, such as nitrate (NO_3^-) reduction to NO_2^- and ammonium oxidation to NO_2^- (Lam et al., 2009). Denitrification, in contrast, is predominantly a heterotrophic process that stepwise reduces NO_3^- to N_2, producing NO_2^-, nitric oxide (NO), and N_2O as intermediates (Devol, 2008). The final step of denitrification, the reduction of N_2O to N_2, is particularly sensitive to oxygen, making complete denitrification more oxygen-sensitive than anammox (Dalsgaard et al., 2014). These differences in substrate dependence and oxygen sensitivity mean that the two N loss pathways occupy distinct niches and respond differently to changes in oxygen concentrations and substrate availability.

Stoichiometric arguments provide a first-order expectation for how the two pathways partition total N loss (Koeve and Kähler, 2010; Babbin et al., 2014; Zakem et al., 2020; Fadum et al., 2025). Under anoxic conditions, denitrification remineralizes organic matter, releasing NH_4^+ as a byproduct. Assuming steady state, organic matter of Redfield composition, and that denitrification is the sole source of NH_4^+ and anammox its sole sink, which is consistent with the absence of NH_4^+ accumulation in OMZs, anammox can sustain at most 29% of total N loss. However, observations rarely match this expected ratio. Instead, one of the two pathways often dominates N loss, and in the ETP in particular, anammox has frequently been found to account for most of the N loss (Kalvelage et al., 2013; Babbin et al., 2017; Karthäuser et al., 2021; Tracey et al., 2023; Cinay et al., 2022). Some studies even attributed all N loss to anammox (Thamdrup et al., 2006; Hamersley et al., 2007).

The reason for the discrepancy between the stoichiometrically expected and observed anammox to denitrification ratio remains unresolved, and several competing explanations have been proposed. One line of reasoning points to additional NH_4^+ sources not captured by the stoichiometric framework, such as dissimilatory nitrate reduction to ammonium (DNRA) (Lam et al., 2009), NH_4^+ excretion from vertically migrating zooplankton (Bianchi et al., 2014), or sedimentary NH_4^+ release (Kalvelage et al., 2013). A second line of reasoning instead suggests that denitrification is systematically underestimated by observations: Dalsgaard et al. (2012) proposed that denitrification occurs only episodically, triggered by pulses of organic matter export, and is therefore often missed by observations, whereas anammox proceeds at a comparatively steady rate. Rate measurement biases are likely to contribute further to the discrepancy (Tracey et al., 2023). Anammox is inherently easier to detect in incubations, as labeled NH_4^+ additions stimulate anammox more strongly than labeled NO_3^- or NO_2^- additions stimulate denitrification, and the low ambient NH_4^+ concentrations result in less dilution of the added label. Additionally, particles are often filtered out or are less likely to be transferred into incubation bottles, removing an important habitat for denitrifying communities. Observations are also concentrated in the oxycline and in nearshore regions, where anammox likely outcompetes denitrification because it tolerates slightly higher oxygen concentrations (Dalsgaard et al., 2014; Zakem et al., 2020). Together,

https://doi.org/10.5194/egusphere-2026-6541
Preprint. Discussion started: 29 October 2026
© Author(s) 2026. CC BY 4.0 License.

these methodological and spatial biases complicate attempts to infer the large-scale balance between the two pathways from observations alone.

Here, we use a high-resolution coupled ocean physical and biogeochemical model of the ETP to resolve anammox and denitrification in a complex, time-dependent environment. This allows us to determine and understand how the processes controlling the two pathways interact with each other and how the anammox to denitrification ratio emerges from these interactions. We identify where the anammox to denitrification ratio varies the most over time, determine on which timescales this variability occurs, and examine which controlling variables underlie this spatiotemporal variability. We hypothesize that the observed fraction of anammox-driven N loss is inflated by the spatial bias of sampling locations, and that when the entire ETP is considered, rather than only the oxyclines and nearshore regions where measurements are concentrated, the anammox to denitrification ratio is closer to the stoichiometrically expected ratio of 29:71. We also test the hypothesis of Dalsgaard et al. (2012), who proposed that the observed contribution of denitrification to N loss is underestimated because denitrification often occurs in short-lived, episodic pulses that are missed by observations. We further examine whether variability in the anammox to denitrification ratio can explain variability in net N_2O production across the ETP.

2 Methods

2.1 Model

To resolve the spatiotemporal variability of the anammox to denitrification ratio, we employ the Regional Ocean Modeling System (ROMS, Shchepetkin and McWilliams, 2005) coupled to the Biogeochemical Elemental Cycling module (BEC, Moore et al., 2001). Our model setup is identical to that described by Härri et al. (2026a) and includes the NitrOMZ module, which explicitly resolves N loss via anammox and denitrification under low-oxygen conditions (Bianchi et al., 2023; McCoy et al., 2023). The telescopic grid configuration spans the entire Pacific Ocean, while providing enhanced resolution in the ETP. Horizontal resolution reaches ∼4 km along the Peruvian coast and gradually coarsens to ∼40 km in the western Pacific, allowing mesoscale eddies to be resolved across most of the ETP. The vertical grid consists of 64 topography-following layers, with refined spacing near the surface and the seafloor. The model was run for 41 years, from January 1979 until December 2019, with a time step of 600 seconds. All of our analyses are based on the daily averaged model output.

The spinup procedure consists of a 20-year physical spinup, followed by a 40-year spinup that includes the BEC and NitrOMZ modules. “Normal” year forcing data was used during the spinup, as described by Köhn et al. (2022). After the spinup, the model was forced at the surface with ERA5 reanalysis data (Hersbach et al., 2020), with corrections to incoming shortwave and outgoing longwave radiation fields based on the Drakkar Forcing Set (DFS5.2) (Dussin et al., 2016). The initial, boundary, and forcing conditions are identical to those described by Köhn et al. (2022) and Härri et al. (2026a).

https://doi.org/10.5194/egusphere-2026-6541
Preprint. Discussion started: 29 October 2026
© Author(s) 2026. CC BY 4.0 License.

2.2 NitrOMZ

The NitrOMZ module explicitly resolves anammox and a three-step denitrification pathway (Bianchi et al., 2023), as illustrated in Fig. 1. It also resolves ammonium oxidation and nitrite oxidation, but does not include DNRA. We discuss the implications of this omission for the anammox to denitrification ratio in Sect. 5. In the following, we describe in detail how anammox and denitrification are implemented in NitrOMZ. For a full description of the NitrOMZ module, we refer to McCoy et al. (2023) and Härri et al. (2026a).

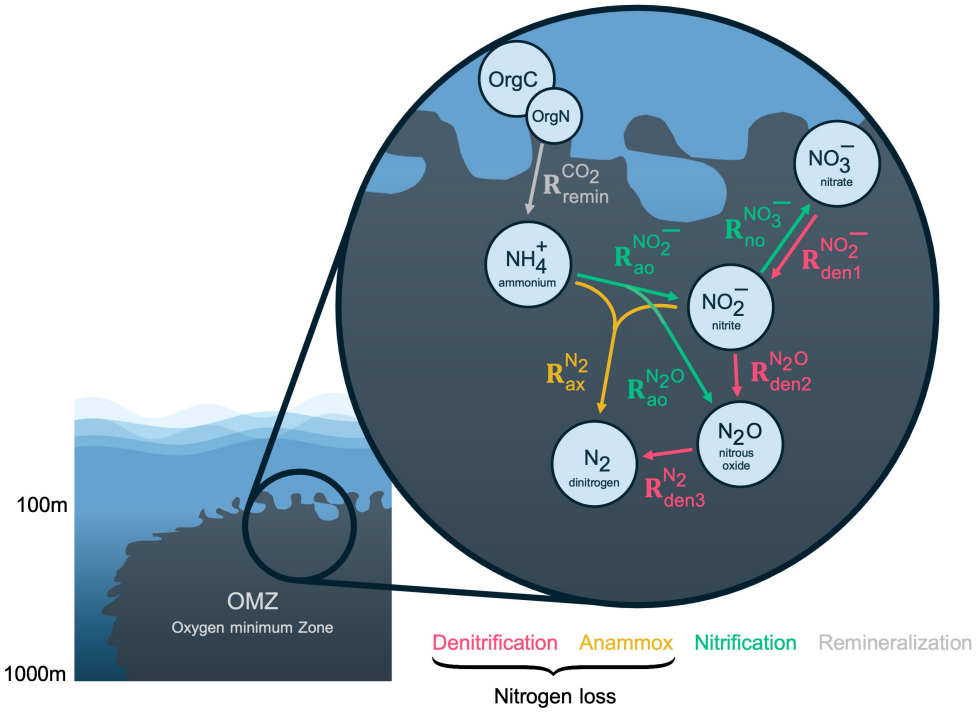


Figure 1. Schematic of the nitrogen cycle resolved by NitrOMZ. The anammox pathway is depicted in yellow ($R^{N_2}_{ax}$). The pink pathways represent the three denitrification steps explicitly considered: (i) nitrate reduction to nitrite ($R^{NO_2^-}_{den1}$), (ii) nitrite reduction to nitrous oxide ($R^{N_2O}_{den2}$), and (iii) nitrous oxide reduction to dinitrogen ($R^{N_2}_{den3}$). The nitrification pathways are shown in green, with ammonium oxidation to both nitrite ($R^{NO_2^-}_{ao}$) and nitrous oxide ($R^{N_2O}_{ao}$) and nitrite oxidation to nitrate ($R^{NO_3^-}_{no}$). Biological uptake of nitrite and air–sea exchange of dinitrogen and nitrous oxide are not shown.

2.2.1 Anammox

Following Dalsgaard et al. (2014) and Bristow et al. (2016), anammox is parameterized in NitrOMZ as a Michaelis–Menten function of the concentrations of NO_2^- and NH_4^+, with additional inhibition by oxygen. The anammox rate, $R^{N_2}_{ax}$, is given by:

https://doi.org/10.5194/egusphere-2026-6541
Preprint. Discussion started: 29 October 2026
© Author(s) 2026. CC BY 4.0 License.

$$R_{ax}^{N_2} = k_{ax} \cdot \frac{[\mathrm{NO_2^-}]}{K_{ax}^{NO_2^-} + [\mathrm{NO_2^-}]} \cdot \frac{[\mathrm{NH_4^+}]}{K_{ax}^{NH_4^+} + [\mathrm{NH_4^+}]} \cdot e^{-\frac{[\mathrm{O_2}]}{K_{ax}^{O_2}}}, \tag{1}$$

where k_{ax} is the maximum anammox reaction rate, $K_{ax}^{NO_2^-}$ and $K_{ax}^{NH_4^+}$ are the half-saturation constants for NO_2^- and NH_4^+, and $K_{ax}^{O_2}$ is the oxygen inhibition constant. The terms $[NO_2^-]$, $[NH_4^+]$, and $[O_2]$ represent the concentrations of the respective tracers. The anammox rate is illustrated as a function of oxygen, NO_2^-, and NH_4^+ in Fig. 2A and 2B, and the parameter values are listed in Table A1.

2.2.2 Denitrification

Denitrification is parameterized in NitrOMZ as a three-step process: NO_3^- is first reduced to NO_2^-, then to N_2O, and finally to biologically unavailable N_2. As a heterotrophic process, denitrification is fueled by organic matter, for which the three denitrification steps compete with aerobic remineralization. To ensure closure of the conservation equation of organic matter in the model, the rate of each denitrification step is computed as a fraction of the total organic matter remineralization rate, R_{remin}^{tot}. In our implementation of ROMS-BEC, R_{remin}^{tot} results from the explicit modeling of particulate organic matter, which is not only sinking, but also being advected and mixed, resulting in complex pathways of organic matter export (Frischknecht et al., 2018).

The fraction of R_{remin}^{tot} attributed to each denitrification step is determined by its pseudo-specific rate, r_H, relative to the sum of the pseudo-specific rates of all four heterotrophic processes. The rate of each denitrification step, R_H^Y, is thus given by:

$$R_H^Y = \frac{r_H}{r_{den1} + r_{den2} + r_{den3} + r_{remin}} \cdot R_{remin}^{tot} \cdot Q_{den}^{N:C}, \tag{2}$$

where H denotes the denitrification step ($H \in \{den1, den2, den3\}$), and Y is its product ($Y \in \{NO_2^-, N_2O, N_2\}$). r_{remin} is the pseudo-specific rate of aerobic remineralization, and $Q_{den}^{N:C}$ is the N:C ratio used to convert the denitrification rates from C units to N units. The pseudo-specific rate of each denitrification step depends on the concentrations of oxygen and its respective substrate, following Dalsgaard et al. (2014), Bristow et al. (2016), and Ji et al. (2018):

$$r_H = k_H \cdot \frac{[\mathrm{X}]}{K_H^X + [\mathrm{X}]} \cdot e^{-\frac{[\mathrm{O_2}]}{K_H^{O_2}}}, \tag{3}$$

where k_H is the maximum rate, $[X]$ the substrate concentration, K_H^X the half-saturation constant for substrate uptake, and $K_H^{O_2}$ the oxygen inhibition constant. The oxygen inhibition constant decreases for successive denitrification steps, making each step more sensitive to oxygen than the previous one. This reflects that the steps are mediated by distinct enzymes and likely by different microorganisms (Körner and Zumft, 1989; Kalvelage et al., 2011; Dalsgaard et al., 2014; Ganesh et al., 2014; Babbin et al., 2015; Ji et al., 2015; Kuypers et al., 2018). The pseudo-specific rate of aerobic remineralization, r_{remin}, is computed similarly, but with oxygen as its substrate, following a Michaelis–Menten dependence on $[O_2]$, and without oxygen inhibition.

https://doi.org/10.5194/egusphere-2026-6541
Preprint. Discussion started: 29 October 2026
© Author(s) 2026. CC BY 4.0 License.

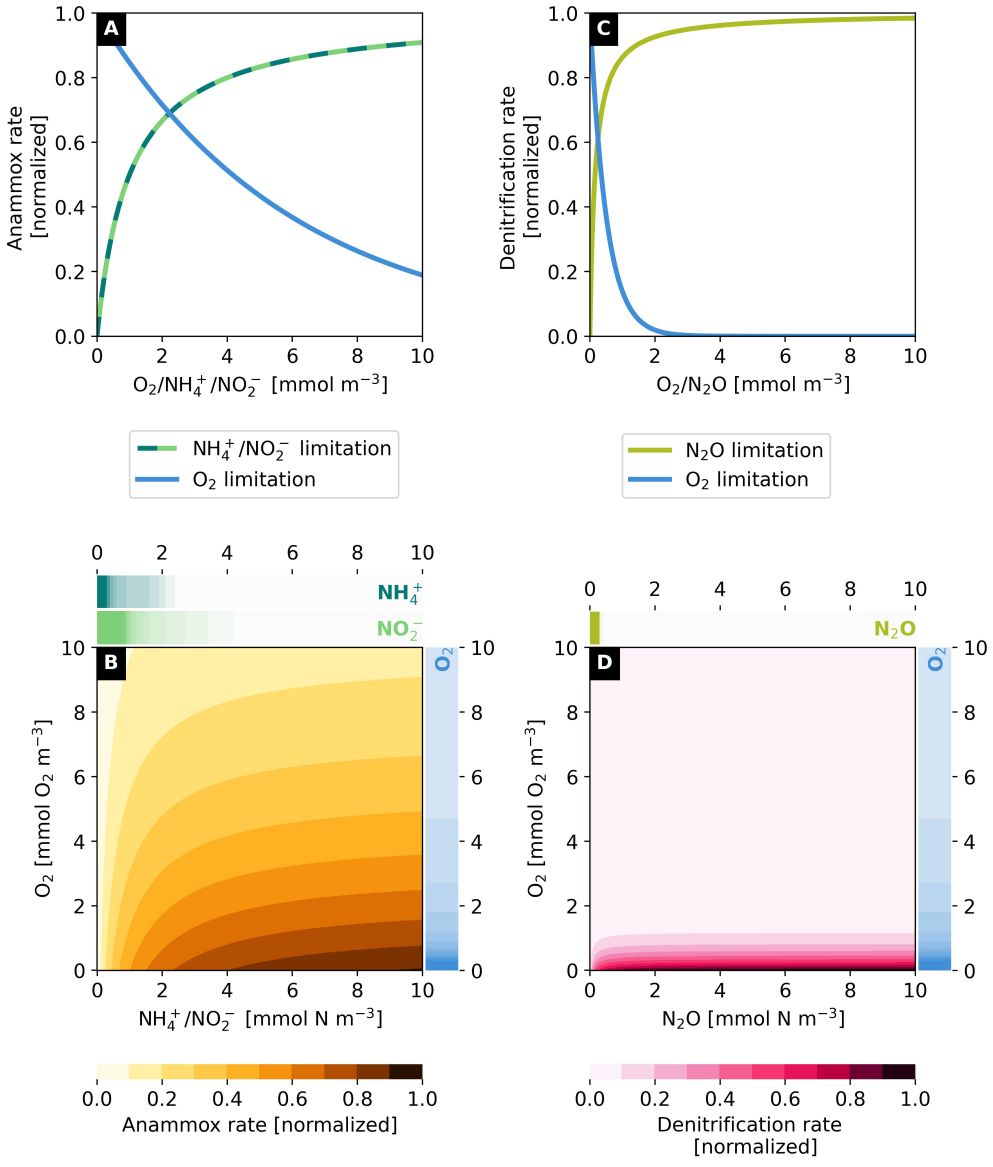


Figure 2. Parameterization of the anammox and denitrification rates in NitrOMZ. (A) Anammox rate as a function of oxygen (O_2) and nitrite (NO_2^-) or ammonium (NH_4^+). (B) Contour plot of the anammox rate as a function of O_2 and NO_2^- or NH_4^+. (C & D) Same as A & B, but for the rate of the last denitrification step as a function of O_2 and nitrous oxide (N_2O). The colorbars indicate the concentrations at which O_2, NO_2^-, N_2O, and NH_4^+ occur in the study region where [O_2] is below 10 mmol O_2 m^{-3} in the 41-year mean, with darker colors indicating higher occurrence.

We use the rate of the last denitrification step, the reduction of N_2O to N_2, to compute the anammox to denitrification ratio. Its rate is shown as a function of oxygen and N_2O in Fig. 2C and 2D, which illustrates that this step is strongly controlled

https://doi.org/10.5194/egusphere-2026-6541
Preprint. Discussion started: 29 October 2026
© Author(s) 2026. CC BY 4.0 License.

by oxygen. This strong oxygen control results from the low oxygen inhibition constant $K_{den3}^{O_2}$, which was derived from experimental estimates (Dalsgaard et al., 2014) and subsequently tuned (Bianchi et al., 2023), making complete denitrification considerably more sensitive to oxygen than anammox. The nitrate and nitrite reduction rates are shown as a function of oxygen and their respective substrates in Fig. A1, and all parameter values are listed in Table A1.

2.3 Analysis Framework

2.3.1 Study Region

To determine the relative contribution of anammox and denitrification to N loss, we focus on the ETP and only consider grid cells where both processes are present in the 41-year mean of our hindcast simulation. Within this volume, we distinguish between three regions based on the mean oxygen concentration: (i) OMZ cores, where [O_2] is below 5 mmol O_2 m^{-3}; (ii) oxyclines, where [O_2] ranges between 5 and 20 mmol O_2 m^{-3}; and (iii) OMZ edges, where [O_2] ranges between 20 and 150

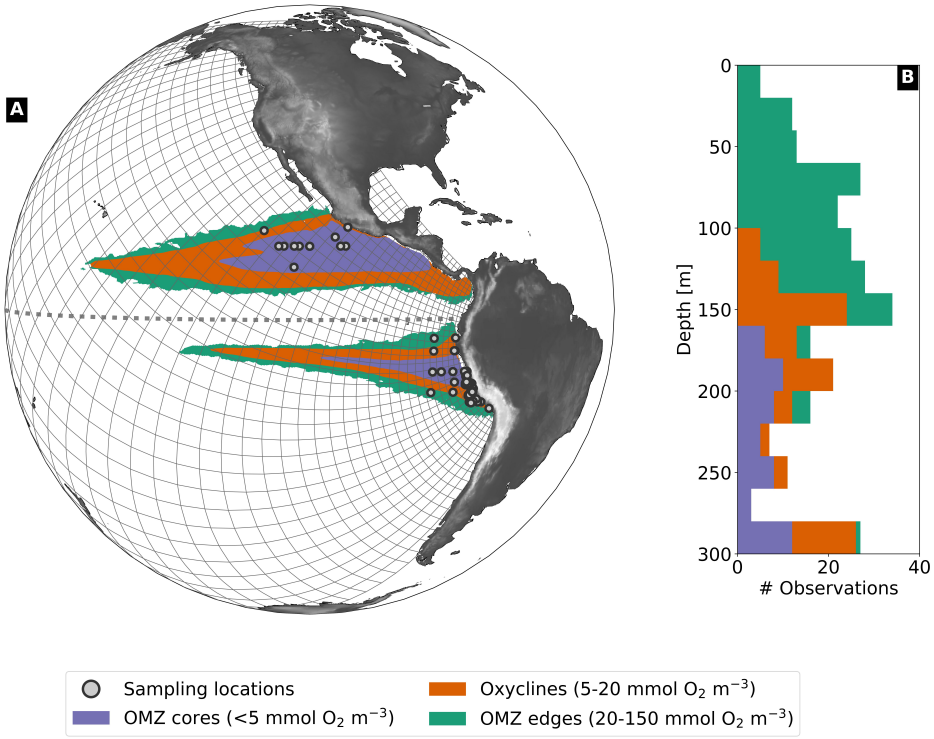


Figure 3. Map of the model domain, study region, and sampling locations. (A) In color, the three regions — OMZ cores, oxyclines, and OMZ edges — used to differentiate parts of the OMZ are shown exemplarily at 200 m depth. Circles indicate sampling locations from Kalvelage et al. (2013), Karthäuser et al. (2021), and Tracey et al. (2023). The dotted line delineates the Eastern Tropical Pacific into a northern and southern part. (B) Distribution of observations by depth, colored by region, assigned based on the 41-year mean modeled oxygen concentration at each sample location.

https://doi.org/10.5194/egusphere-2026-6541
Preprint. Discussion started: 29 October 2026
© Author(s) 2026. CC BY 4.0 License.

mmol O_2 m^{-3}. These three regions are shown exemplarily at 200 m depth in Fig. 3A. For some analyses, we further distinguish between the northern OMZ, located in the Eastern Tropical North Pacific (ETNP), and the southern OMZ, located in the Eastern Tropical South Pacific (ETSP), which we separate at the equator. Although the OMZ core extends from approximately 150 to 1200 m depth in the model, we restrict all analyses beyond the model evaluation to the upper 300 m, using data interpolated from ROMS' sigma layers onto regular depth levels with a 20 m vertical resolution. We focus on this depth range because (i) most of the spatiotemporal variability in N loss occurs there, (ii) most observational studies reporting anammox and denitrification rates have concentrated on this depth range (Kalvelage et al., 2013; Karthäuser et al., 2021; Tracey et al., 2023), and (iii) it keeps the analysis of daily output over 41 years computationally feasible.

2.3.2 Comparison to Observations

We compare simulated anammox and denitrification rates to observations from Kalvelage et al. (2013), Karthäuser et al. (2021), and Tracey et al. (2023). We consider all observations from the top 300 m, corresponding to 270 of the 309 total observations. Of these, we exclude three observations with denitrification rates close to or exceeding 1000 µmol N m^{-3} d^{-1}, as we consider them outliers, given that they exceed the maximum of all other observations more than fivefold. This leaves 267 observations for the comparison. For each observation, we subsample the model on the same day, depth, and location, averaging over all grid cells within a 0.25° radius. Most observations are located in the top 150 m and fall within the oxyclines or OMZ edges (Fig. 3B). All three studies determined anammox and denitrification rates by incubating samples with isotopically labeled substrates. However, sampling protocols and substrate additions varied between studies, limiting their direct comparability. Nevertheless, these studies provide the most comprehensive set of paired anammox and denitrification rate measurements in the ETP, and there is no straightforward way to standardize them across studies.

2.3.3 Definition of the Anammox to Denitrification Ratio

To compute the anammox to denitrification ratio for a given region and period, we first integrate anammox and denitrification rates over the relevant volume V and time interval (t_1 to t_2), and then calculate the fraction of N loss driven by anammox (f_{ax}) from these integrals:

$$f_{ax} = \frac{\int_V \int_{t_1}^{t_2} R_{ax}^{N_2} \, \mathrm{d}t \, \mathrm{d}V}{\int_V \int_{t_1}^{t_2} R_{ax}^{N_2} \, \mathrm{d}t \, \mathrm{d}V + \int_V \int_{t_1}^{t_2} R_{den3}^{N_2} \, \mathrm{d}t \, \mathrm{d}V}. \tag{4}$$

Here, $R_{ax}^{N_2}$ denotes the local anammox rate, $R_{den3}^{N_2}$ the rate of the last denitrification step, which yields N_2, and V the volume of integration relevant to each analysis. f_{ax} ranges from 0 (N loss entirely driven by denitrification) to 1 (N loss entirely driven by anammox). In the text, we report the anammox to denitrification ratio as $100 \cdot f_{ax} : 100 \cdot (1 - f_{ax})$, whereas figures show f_{ax} directly.

Integrating rates over space and time before computing the ratio is equivalent to computing an N-loss-weighted ratio. It ensures that grid cells and periods with high N loss rates contribute more strongly to the ratio than those where N loss is neg-

https://doi.org/10.5194/egusphere-2026-6541
Preprint. Discussion started: 29 October 2026
© Author(s) 2026. CC BY 4.0 License.

ligible. This avoids biases from ratios in grid cells or at time steps with near-zero N loss. Because high N loss rates typically co-occur with a low anammox to denitrification ratio, whereas anammox dominates at slightly elevated oxygen concentrations where total N loss is low, this weighting gives more weight to denitrification-dominated grid cells and periods. As a consequence, a ratio integrated over space is more sensitive to regional excursions toward a lower anammox to denitrification ratio than toward a higher one, and a ratio integrated over time is more sensitive to short periods of denitrification-dominated N loss than to periods dominated by anammox.

2.3.4 Time Series Decomposition

To determine on which timescales variability occurs in the anammox to denitrification ratio, we applied a seasonal-trend decomposition using LOESS (STL), as implemented in the Python function `STL` from `statsmodels.tsa.seasonal`. For spatially resolved analyses, we applied STL directly to the time series of the ratio at each grid cell. For spatially integrated analyses, we first computed a single time series of the ratio and then applied STL to it. In both cases, STL decomposes the time series into a trend, a seasonal, and a residual component, which we hereafter refer to as the interannual (I), seasonal (S), and subseasonal (R) components, respectively. The subseasonal component thus comprises all variability not captured by the trend or the mean seasonal cycle. To illustrate the relative importance of each timescale, we calculated the fraction of total variability captured by each component, $C \in \{I, S, R\}$, as:

$$f_C = \frac{\mathrm{Var}(C)}{\mathrm{Var}(I) + \mathrm{Var}(S) + \mathrm{Var}(R)}, \tag{5}$$

where $\mathrm{Var}(C)$ denotes the variance of component C over the analysis period.

2.3.5 Controlling Variables of the Anammox to Denitrification Ratio

In order to develop a better understanding of what controls the anammox to denitrification ratio, we examine how this ratio varies as a function of each of the six different controlling variables: O_2, NO_2^-, NH_4^+, N_2O, NO_3^-, and the rate of remineralization. To keep things simple, we only analyze the local partial dependence. This means that while we vary the value of the controlling variable of interest, we hold all other controlling variables constant at a reference value, given by their N-loss-weighted median across all grid cells where both anammox and denitrification are present in the model. We thus explicitly neglect the potential covariations between the variables in nature and in the model. To illustrate how sensitive the anammox to denitrification ratio is to the values of the other controlling variables, we repeat this analysis for five reference values of each of the other controlling variables, spanning their 45th to 55th percentiles, and compute the ratio for every combination. The resulting response curves are shown in Fig. 4, with shading indicating the range of responses across all combinations, which reflects interactions between the controlling variables. The underlying responses of the anammox and denitrification rates to each controlling variable are shown in the appendix (Fig. A2).

In this idealized setting, oxygen controls the ratio most strongly, except under fully anoxic conditions. At $[O_2] = 0$, oxygen inhibition plays no role, and the ratio of roughly 27:73 depends fully on the other controlling variables. The ratio then increases

https://doi.org/10.5194/egusphere-2026-6541
Preprint. Discussion started: 29 October 2026
© Author(s) 2026. CC BY 4.0 License.

rapidly with oxygen and reaches values close to 100:0 at around 4 mmol O_2 m^{-3}. At the same time, increases in [NO_2^-] and [NH_4^+] raise the ratio, while increases in [N_2O] and the remineralization rate lower it, but these effects diminish with increasing oxygen. The dominant role of oxygen is also apparent from the shading in Fig. 4: the response curves of all other controlling variables show a wide spread, which results mainly from varying [O_2] within its 45th–55th percentiles, whereas the oxygen response curve shows hardly any visible spread.

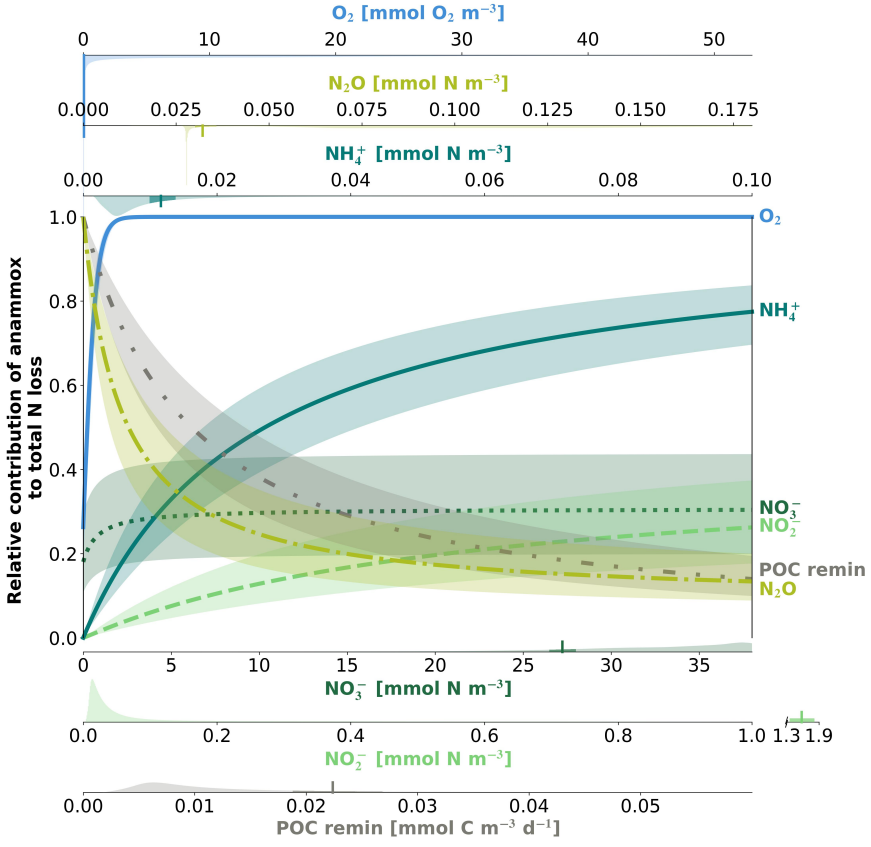


Figure 4. Idealized analysis of the dependence of the anammox to denitrification ratio on the six controlling variables. Each line shows, for one variable at a time, how the ratio changes as that variable varies. The other variables were fixed at five reference values spanning their nitrogen-loss-weighted 45th–55th percentiles, including the median, and the response was computed for every combination. The thick line gives the median response and the shading the minimum-to-maximum range across all combinations. Controlling variables are shown from 0 to their 90th percentile, taking into account only regions where anammox and denitrification are present in the 41-year mean. The histogram on each axis shows that variable's distribution across these regions. The darker histogram bars and vertical line mark the nitrogen-loss-weighted 45th–55th percentile range and median of that variable. Due to computational constraints, only every 5th day and every 3rd grid cell was considered.

https://doi.org/10.5194/egusphere-2026-6541
Preprint. Discussion started: 29 October 2026
© Author(s) 2026. CC BY 4.0 License.

Assuming each controlling variable exhibits comparable relative variability and no strong covariations, we expect oxygen to be the dominant control on the spatiotemporal variability of the ratio, structuring it spatially, with a lower ratio in the OMZ cores and a higher ratio at the OMZ edges, and accounting for most of its variability over time. This strong oxygen control arises from the exponential oxygen inhibition in our parameterization, in which the oxygen inhibition constant of the last denitrification step ($K_{den3}^{O_2}$ = 0.506 mmol O_2 m^{-3}) is considerably smaller than that of anammox ($K_{ax}^{O_2}$ = 6 mmol O_2 m^{-3}). As a result, denitrification rates decline much more rapidly with increasing oxygen than anammox rates (Fig. 2). We discuss the uncertainty of both constants and their implications for the anammox to denitrification ratio in Sect. 5.

While this idealized analysis provides a first indication of the main controls on the ratio, strong covariations and feedbacks could alter these conclusions. For example, remineralization not only fuels denitrification but also releases NH_4^+, and can thus enhance both anammox and denitrification (Kalvelage et al., 2013). Moreover, substrate concentrations and remineralization shift the ratio only slightly once oxygen rises above zero, but the idealized analysis holds them close to their median. Larger simultaneous changes in substrate supply and remineralization could add up to an effect that rivals that of oxygen. This is where the full dynamics of the simulation become crucial.

3 Evaluation of Anammox and Denitrification Rates

Integrated over the entire water column and averaged over the 41-year simulation, the model estimates a total N loss of 84.7 Tg N y^{-1} for the ETP, slightly exceeding previous estimates of 39–70 Tg N y^{-1} (Deutsch et al., 2001; Bianchi et al., 2012; DeVries et al., 2013; Yang et al., 2017). Of this, a bit less than half, namely 36.6 Tg N y^{-1}, is lost within the upper 300 m.

Of the 36.6 Tg N y^{-1} lost in the upper 300 m, anammox contributes 5.4 Tg N y^{-1} in the ETSP and 8.3 Tg N y^{-1} in the ETNP, while denitrification contributes 8.5 Tg N y^{-1} in the ETSP and 14.4 Tg N y^{-1} in the ETNP. Of these estimates, we can only compare anammox-driven N loss in the ETSP to observations, as comparable estimates for the ETNP or for denitrification are unavailable. Extrapolations of observations over the entire water column of the ETSP suggest that anammox removes about 10 Tg N y^{-1} (Kalvelage et al., 2013). Integration over the entire water column of the ETSP raises our estimate to 12.7 Tg N y^{-1}, which is close to the observation-based estimate and indicates that the model reproduces realistic anammox-driven N loss, at least in the ETSP.

The temporally averaged spatial pattern of anammox reveals the highest rates along the Central American and Peruvian coasts (Fig. 5A–C, shown exemplarily at 200 m), reaching almost 100 µmol N m^{-3} d^{-1} in the top 300 m in the 41-year mean. Anammox rates decline by several orders of magnitude with distance from shore (Fig. 5D, Fig. A3A–C). Within the region sampled by Kalvelage et al. (2013), both the model and observations show a decline of about two orders of magnitude in depth-integrated anammox rates from east to west. Across the full simulation period, modeled anammox rates range from 0 to 507 µmol N m^{-3} d^{-1}, encompassing the range of 3–279 µmol N m^{-3} d^{-1} observed by Lam et al. (2009) and Kalvelage et al. (2013), with higher modeled maxima expected, as the model covers the entire ETP at daily resolution over 41 years. Vertically, anammox rates peak around 100 m depth (Fig. 5E), consistent with observed peak anammox rates in the oxyclines (Lam et al., 2009; Tracey et al., 2023).

https://doi.org/10.5194/egusphere-2026-6541
Preprint. Discussion started: 29 October 2026
© Author(s) 2026. CC BY 4.0 License.

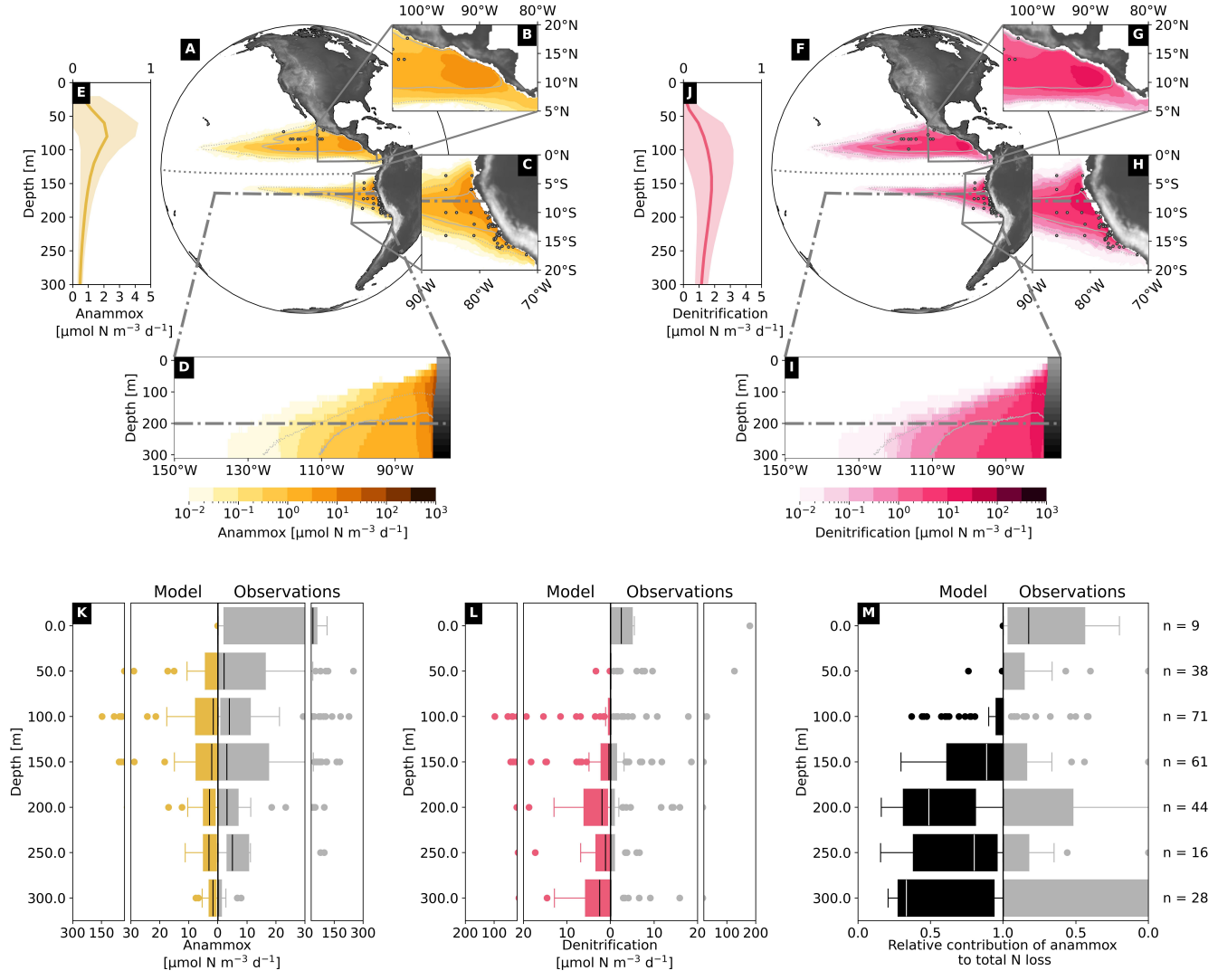


Figure 5. Evaluation of anammox and denitrification rates. (A) Anammox rates averaged over 41 years at 200 m, with circles indicating sampling locations; (B) and (C) show zooms of the northern and southern Eastern Tropical Pacific, respectively. (D) Anammox rates along the 8°S transect. (E) Depth profile of anammox rates averaged over the regions where both anammox and denitrification are present in the model; shading indicates the standard deviation over time of the spatially averaged rates over 41 years. (F–J) Same as (A–E), but for denitrification rates. The solid and dotted contours depict the 5 and 20 mmol O_2 m^{-3} thresholds in the 41-year mean, respectively, delineating the boundaries between the OMZ cores, oxyclines, and OMZ edges. Comparison of observed and modeled (K) anammox rates, (L) denitrification rates, and (M) fraction of anammox-driven nitrogen loss (f_{ax}), with lines depicting the median. Modeled values are shown on the left of each subplot and measurements on the right, with greater symmetry indicating better agreement between observations and model. Observations were compiled from Kalvelage et al. (2013), Karthäuser et al. (2021), and Tracey et al. (2023).

https://doi.org/10.5194/egusphere-2026-6541
Preprint. Discussion started: 29 October 2026
© Author(s) 2026. CC BY 4.0 License.

Temporally averaged denitrification rates exhibit a similar spatial pattern, peaking along the Central American and Peruvian coasts (Fig. 5F–H, shown exemplarily at 200 m), though slightly more offshore than anammox, reaching almost 60 µmol N m^{-3} d^{-1} in the top 300 m in the 41-year mean. Similarly to anammox rates, denitrification rates decline with distance from shore (Fig. 5I, Fig. A3D–F). Throughout the full simulation period, modeled denitrification rates range from 0 to 8682 µmol N m^{-3} d^{-1} — far exceeding the time-averaged peak of 60 µmol N m^{-3} d^{-1} — indicating that such extreme values occur only briefly. Vertically, denitrification rates peak slightly deeper than anammox rates, between 150 and 200 m depth (Fig. 5J). This vertical separation of anammox and denitrification is consistent with Babbin et al. (2017), who found that anammox drives more than 50% of total N loss in the top 150 m, while denitrification becomes increasingly important below. It also agrees with the finding that anammox persists at higher oxygen concentrations than denitrification (Dalsgaard et al., 2014; Zakem et al., 2020).

Observed and individually subsampled modeled anammox rates are significantly correlated ($r = 0.46$, $p < 0.05$). In contrast, no such correlation exists for denitrification rates, likely because both observations and the model show non-zero denitrification rates only sporadically. Because such a point-to-point comparison is subject to several scale mismatches — for example, the model output represents a daily average over a 0.25° radius and 20 m depth interval — we additionally compare observed and modeled rates across depth bins (Fig. 5K & L). This comparison shows that the model captures a similar depth distribution for both anammox and denitrification rates, including the spread in rates at different depth intervals. The model also reproduces the anammox-dominated N loss observed at sampling locations, with a similar decrease in the relative contribution of anammox to N loss with depth (Fig. 5M). Averaging the ratio computed for each sample yields an observed value of 83:17, with an interquartile range from 82:18 to 100:0, compared to a modeled value of 78:22, with an interquartile range from 56:44 to 100:0. When weighting each sample by its N loss rate instead (Eq. 4), the discrepancy between model and observations increases, with a modeled ratio of 63:37 compared to an observed ratio of 86:14. This weighting by N loss lowers the anammox share in the model, where high N loss rates coincide with denitrification, but not in the observations, where the highest N loss rates are dominated by anammox, possibly reflecting measurement biases favoring the detection of anammox (Tracey et al., 2023). Computing the ratio from the 41-year mean rates at each sampling location instead of the subsampled model output lowers the modeled ratio further, to 60:40 when averaging across sampling locations and to 54:46 when weighting each location by its N loss rate. This indicates that discrete sampling might miss denitrification pulses, as hypothesized by Dalsgaard et al. (2012).

4 Results and Discussion

4.1 Comparison of the Local and ETP-wide Anammox to Denitrification Ratio

In strong contrast to the anammox-dominated N loss at the sampling locations described in Sect. 3, the extension of the analysis to the entire ETP reveals a system where N loss is dominated by denitrification with an anammox to denitrification ratio of 37:63. Concretely, anammox and denitrification contribute 13.7 and 22.9 Tg N y^{-1}, respectively, to the 36.6 Tg N y^{-1} lost in the top 300 m. The anammox to denitrification ratio is slightly higher in the ETSP, at 39:61, than in the ETNP, at 37:63, but denitrification drives the majority of N loss in the top 300 m in both regions. Integrated over the entire water column, the ETP-wide ratio decreases further to 32:68. This ratio is far closer to the stoichiometrically expected ratio than to the anammox-

https://doi.org/10.5194/egusphere-2026-6541
Preprint. Discussion started: 29 October 2026
© Author(s) 2026. CC BY 4.0 License.

dominated N loss reported by most observational studies (Thamdrup et al., 2006; Hamersley et al., 2007; Kalvelage et al., 2013; Babbin et al., 2017; Karthäuser et al., 2021; Tracey et al., 2023; Cinay et al., 2022).

The comparison of the anammox to denitrification ratio at sampling locations and across the entire ETP supports our hypothesis: spatial, and to a lesser extent temporal, biases in sampling lead to an overestimation of the relative contribution of anammox to N loss when observations are taken as representative of the ETP. Once these sampling biases are accounted for, the apparent mismatch between stoichiometric expectations and observations resolves: observations capture the anammox-dominated N loss at sampling locations but are not representative of the ratio across the ETP as a whole. Our results, therefore, highlight that broader spatial sampling coverage, combined with repeated sampling over time, is needed to resolve the ETP-wide balance between the two pathways.

We next examine the spatial pattern of the anammox to denitrification ratio and its temporal variability to identify where broader sampling is most needed to resolve the ETP-wide balance between anammox and denitrification, and to identify regions of high temporal variability, where pulses in denitrification are most likely to cause snapshot measurements to miss the long-term balance between the two pathways.

4.2 Spatial and Temporal Variability in the Anammox to Denitrification Ratio

The spatial structure of the anammox to denitrification ratio closely follows oxygen concentrations within the OMZs, as shown exemplarily at 200 m (Fig. 6A–C) and along the 8°S transect (Fig. 6D). In the OMZ cores, denitrification dominates, contributing more than 70% of N loss (Fig. 6A–D). The fraction of anammox-driven N loss increases gradually toward the edges of the OMZs, where anammox drives almost 100% of the N loss, consistent with the idealized oxygen dependence of the anammox to denitrification ratio shown in Fig. 4. However, absolute N loss at the OMZ edges is low (Fig. 5), meaning that this strong anammox dominance contributes little to total N loss across the ETP.

This spatial structure of the anammox to denitrification ratio is consistent with previous studies showing that anammox persists at higher oxygen levels than denitrification (Dalsgaard et al., 2014; Zakem et al., 2020). The oxygen dependence of the ratio remains visible even when we compute the depth-resolved anammox to denitrification ratio from spatially integrated anammox and denitrification rates (Fig. 6E). Anammox drives more than half of the total N loss in the top 150 m, where oxygen concentrations are higher, while denitrification drives the majority of N loss below 150 m, where oxygen concentrations are lower. This vertical switch is consistent with the depth distribution of anammox and denitrification rates described in Sect. 3 and with observations by Babbin et al. (2017).

Temporal variability in the anammox to denitrification ratio is highest in the oxyclines, where mean oxygen concentrations range between 5 and 20 mmol O_2 m^{-3}. There, the standard deviation of the anammox to denitrification ratio reaches 0.5, meaning the ratio can swing across the full range from entirely anammox- to entirely denitrification-driven N loss (Fig. 6F–I). In the OMZ cores and at the OMZ edges, variability is much lower, reaching a standard deviation of at most 0.2. When we depth-resolve the temporal variability by computing the standard deviation of the ratio from spatially integrated rates (Fig. 6J), we partially retain this pattern: variability is highest in the top 150 m, where oxygen concentrations are higher, and remains low at greater depths, consistent with persistently near-anoxic conditions there. The low variability we find at the OMZ edges,

https://doi.org/10.5194/egusphere-2026-6541
Preprint. Discussion started: 29 October 2026
© Author(s) 2026. CC BY 4.0 License.

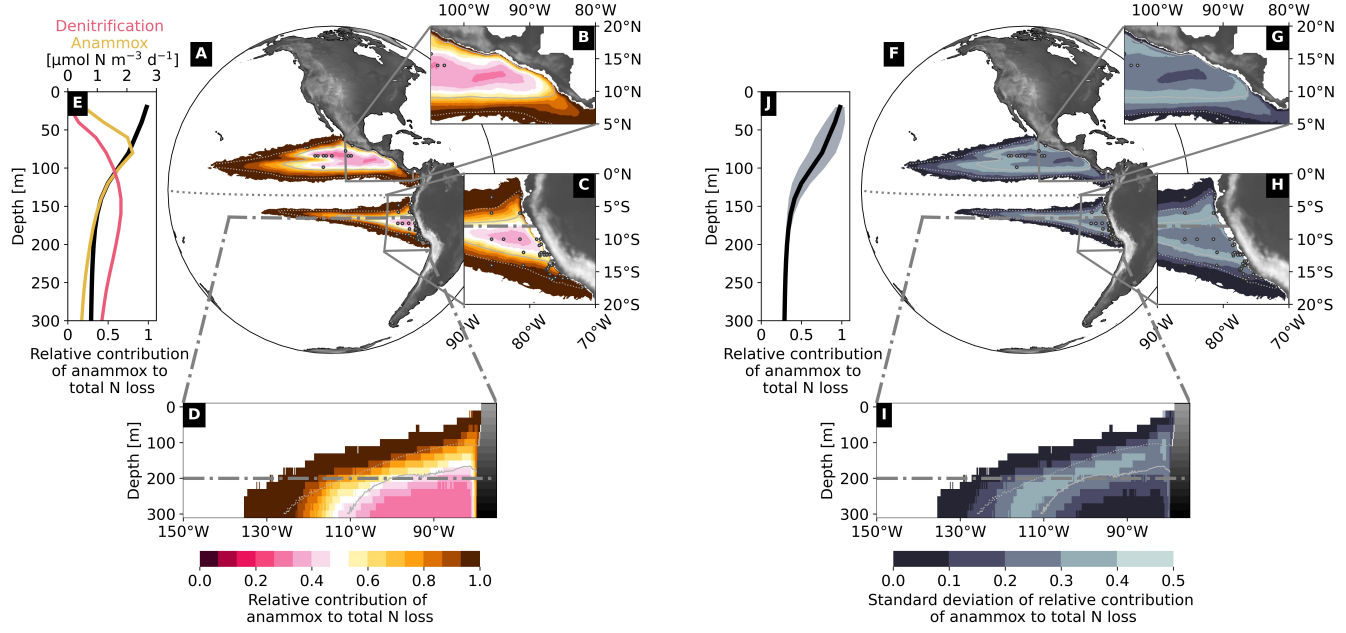


Figure 6. Spatial and temporal variability in the anammox to denitrification ratio. (A) Fraction of anammox-driven nitrogen loss (f_{ax}), computed from rates integrated over 41 years, at 200 m, with circles indicating sampling locations; (B) and (C) show zooms of the northern and southern Eastern Tropical Pacific, respectively. (D) f_{ax} along the 8°S transect. (E) Depth profile of f_{ax}, anammox rates, and denitrification rates, computed from rates integrated over the regions where both anammox and denitrification are present in the model. (F–I) Same as (A–D), but for the temporal standard deviation of the daily f_{ax} over the 41 years. (J) Depth profile of f_{ax}, with shading indicating its temporal standard deviation over the 41 years. The solid and dotted contours depict the 5 and 20 mmol O_2 m^{-3} thresholds in the 41-year mean, respectively, delineating the boundaries between the OMZ cores, oxyclines, and OMZ edges.

however, is not reflected in the depth-resolved variability, likely because N loss rates there are low and contribute little to the spatially integrated signal.

These findings carry three implications for how N loss observations should be collected and interpreted when used to infer the long-term balance between anammox and denitrification. First, they reinforce our earlier finding that most measurements were taken in regions where anammox dominates N loss. This likely reflects a focus on regions of high N cycling activity, which are well suited to studying the processes and organisms involved, as well as logistical constraints that favor sampling close to the coast. As a result, the mean of all observations is strongly biased toward anammox compared to the ETP-wide ratio. Capturing the ETP-wide ratio therefore requires sampling locations that span the full range of oxygen concentrations found within OMZs, including the OMZ cores. Second, individual measurements likely do not represent the temporal mean either, because the ratio also varies strongly over time. This is particularly true in the oxyclines, where N loss swings between fully anammox-driven and fully denitrification-driven, and where about a third of all observations were taken (Fig. 3B). Capturing the long-term ratio therefore requires repeated sampling at the same location. Third, given the strong link between the ratio and

https://doi.org/10.5194/egusphere-2026-6541
Preprint. Discussion started: 29 October 2026
© Author(s) 2026. CC BY 4.0 License.

oxygen concentration, measurements should always be interpreted together with the in situ oxygen concentration, as this may shape the ratio at a given snapshot in time more strongly than the sampling location itself. This oxygen dependence also has consequences for incubation experiments: if oxygen concentrations are not maintained at their in situ level during sampling or incubation, measured rates could be biased toward one pathway, which is a known technical challenge (Garcia-Robledo et al., 2021).

So far, we have identified where the anammox to denitrification ratio varies over time, but not on which timescales this variability occurs. Since short-lived denitrification pulses (Dalsgaard et al., 2012) would appear as subseasonal variability, identifying where this timescale dominates allows us to assess where snapshot measurements are most likely to miss such pulses. The timescales of variability also indicate how often a location needs to be sampled to capture its long-term mean.

4.3 Timescales of Variability in the Anammox to Denitrification Ratio

The decomposition of the time series of the anammox to denitrification ratio into subseasonal, seasonal, and interannual components reveals a low contribution of the seasonal timescale overall, but distinct differences between the regions of the OMZ. In the OMZ cores and at the OMZ edges, subseasonal variability dominates, explaining more than 80% of the variability, whereas in the oxyclines, interannual variability dominates, explaining more than 80%.

Subseasonal changes are responsible for most of the temporal variability in the anammox to denitrification ratio in both the OMZ cores and at the OMZ edges (Fig. 7A & B). The magnitude of this subseasonal variability differs markedly between the two regions: in the OMZ cores, the ratio stays within a narrow 27:73 to 37:63 range, while at the OMZ edges, it swings between 34:66 and 100:0 (Fig. 7C & D), although such excursions are brief, consistent with the low standard deviation at the OMZ edges (Fig. 6F–I). Note, however, that because the spatially integrated ratio is N-loss-weighted (Sect. 2.3.3), brief excursions toward more anammox-dominated ratios in the OMZ cores may be underrepresented, so local variability could be higher than the time series suggest.

On seasonal timescales, the anammox to denitrification ratio shows only weak variability, mostly confined to coastal upwelling regions (Fig. 7E & F), possibly related to seasonal changes in upwelling. In both the ETNP and the ETSP, the ratio is higher during the respective local winter and lower during local summer. Seasonal variability in the ratio is most pronounced at the OMZ edges (Fig. 7G & H).

Interannual changes are responsible for most of the temporal variability in the anammox to denitrification ratio in the oxyclines (Fig. 7I & J), although variability on interannual timescales is also present at the OMZ edges (Fig. 7K & L). Much of this interannual variability can be attributed to the El Niño–Southern Oscillation (ENSO), as indicated by a significant positive correlation between the ratio and the ENSO index in each region ($p < 0.05$). During El Niño events, the relative contribution of anammox increases, while during La Niña events, the relative contribution of denitrification increases. The ENSO-driven variability in the anammox to denitrification ratio coincides with changes in total N loss in the top 300 m, which decreases by $\sim$11 Tg N y^{-1} during El Niño and increases by a similar magnitude during La Niña (Figs. A4K & L, A5K & L). This ENSO-driven change in N loss is comparable to the $\sim$13 Tg N y^{-1} estimated by Yang et al. (2017) for the entire water column,

https://doi.org/10.5194/egusphere-2026-6541
Preprint. Discussion started: 29 October 2026
© Author(s) 2026. CC BY 4.0 License.

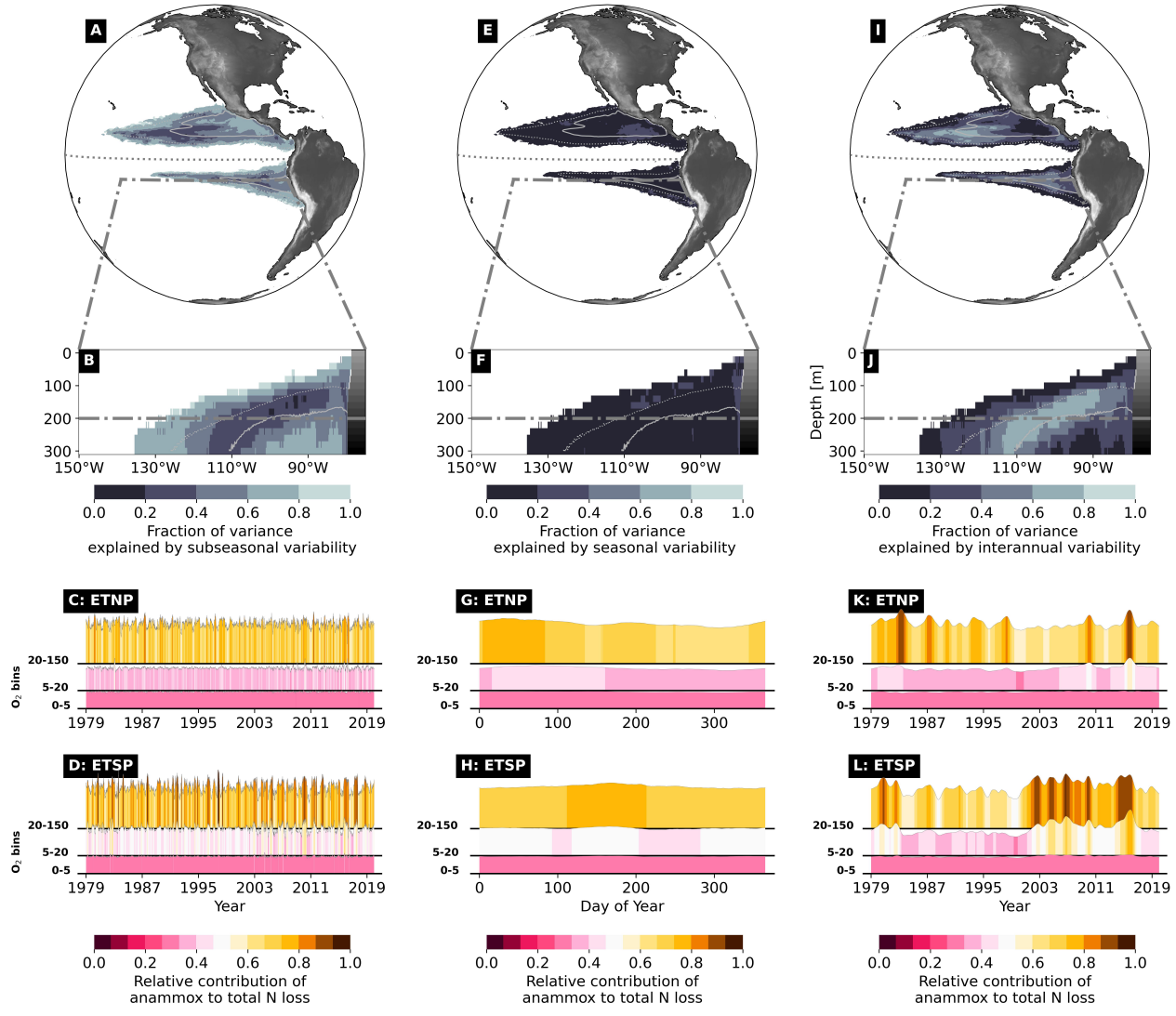


Figure 7. Subseasonal, seasonal, and interannual variability in the anammox to denitrification ratio. Panels (A) and (B) show the fraction of variability explained by subseasonal variability at 200 m and along the 8°S transect, respectively. Panels (C) and (D) show subseasonal variability in the OMZ cores, oxyclines, and OMZ edges of the ETNP and ETSP, respectively. Panels (E–H) and (I–L) show the same decomposition for seasonal and interannual variability, respectively. The solid and dotted contours depict the 5 and 20 mmol O_2 m^{-3} thresholds in the 41-year mean, respectively, delineating the boundaries between the OMZ cores, oxyclines, and OMZ edges.

suggesting that our estimate for the top 300 m, where most of the variability occurs, captures the bulk of the ENSO-driven variability in N loss.

Interestingly, Mogollón and Calil (2017) found the opposite relationship between the anammox to denitrification ratio and ENSO for the coastal ETSP, with anammox dominating during La Niña and denitrification during El Niño. We recover this

https://doi.org/10.5194/egusphere-2026-6541
Preprint. Discussion started: 29 October 2026
© Author(s) 2026. CC BY 4.0 License.

opposite relationship when computing the ratio across the entire ETP without distinguishing between the regions of the OMZ: while the ratio correlates positively with the ENSO index within each region, it correlates negatively when integrated across all regions. This reversal arises because ENSO also changes the relative contribution of each region to total N loss, so that the integrated ratio can shift in the opposite direction from the ratio within each region. This underscores the importance of resolving the ratio separately across different parts of the OMZ.

In summary, the anammox to denitrification ratio and its timescales of variability follow a layered, onion-like spatial pattern. In the OMZ cores, where mean oxygen concentrations remain below 5 mmol O_2 m^{-3}, total N loss rates are highest and largely driven by denitrification. Temporal variability here is weak and occurs mainly on subseasonal timescales. Moving outward to the oxyclines, where mean oxygen concentrations range between 5 and 20 mmol O_2 m^{-3}, the fraction of anammox-driven N loss increases, and temporal variability in the ratio is highest, occurring mainly on interannual timescales. At the OMZ edges, where mean oxygen concentrations range between 20 and 150 mmol O_2 m^{-3}, N loss is anammox-dominated, but total N loss rates are small. Temporal variability here is again weak and occurs mainly on subseasonal timescales, though a non-negligible interannual signal is also present.

For observations, our findings have different implications for each region. In the OMZ cores, the ratio varies mainly on subseasonal timescales, so repeated measurements over a single year that resolve this variability likely suffice to capture its long-term mean. In the oxyclines, multi-year measurements are needed to capture the long-term ratio because the ratio varies on interannual timescales. At the OMZ edges, non-negligible variability of the ratio on interannual timescales similarly calls for multi-year measurements. Additionally, high-frequency sampling might be especially relevant at the OMZ edges, since the dominant subseasonal variability there may be driven by short-lived denitrification pulses, which, if missed, lead to an overestimation of the contribution of anammox to N loss.

In the following, we identify the controlling variables of the spatiotemporal variability in the anammox to denitrification ratio in more detail. Identifying the dominant control may matter beyond the ratio itself. The last denitrification step, which we use to compute this ratio, consumes N_2O and is more oxygen-sensitive than the step that produces it. This mirrors the difference in oxygen sensitivity between this last step and anammox (Dalsgaard et al., 2014). If oxygen is the dominant controlling variable, the anammox to denitrification ratio might therefore covary positively with net N_2O production.

4.4 Controls on Variability in the Anammox to Denitrification Ratio

Extending the idealized analysis described in Sect. 2.3.5, we compute the ratio at the 10th to 90th percentiles of each controlling variable for each region, while holding all other controlling variables at their regional median (Fig. 8). This reveals oxygen as the dominant control on the anammox to denitrification ratio in all three regions of the OMZ. In the OMZ cores, variability in [O_2] has the largest effect on variability in the ratio, followed by variability in [NO_2^-] and [N_2O] (Fig. 8A & B). The interquartile range of [O_2] spans only 0 to 3 mmol O_2 m^{-3}, but this range falls exactly where the response of the ratio to [O_2] is steepest (Fig. 4). While [O_2] thus sets the baseline of the ratio, variability in [NO_2^-], [N_2O], [NH_4^+], and remineralization modulates it slightly in either direction, an effect that becomes stronger the lower [O_2] is.

https://doi.org/10.5194/egusphere-2026-6541
Preprint. Discussion started: 29 October 2026
© Author(s) 2026. CC BY 4.0 License.

In the oxyclines and at the OMZ edges, the median $[O_2]$ exceeds 10 mmol O_2 m^{-3} in both regions (Fig. 8C–F). In the absence of variability in $[O_2]$, such high concentrations would keep N loss fully anammox-dominated, albeit at extremely low absolute rates. Spatiotemporal variability in $[O_2]$ is therefore the primary controlling variable of variability in the ratio in these regions as well. However, whenever $[O_2]$ drops toward near-zero, $[NO_2^-]$, $[N_2O]$, $[NH_4^+]$, and remineralization play the same secondary role in shaping the ratio as identified for the OMZ cores. Such near-zero oxygen excursions occur regularly in both regions, as reflected in the large variability in $[O_2]$ shown in Fig. 8C & E.

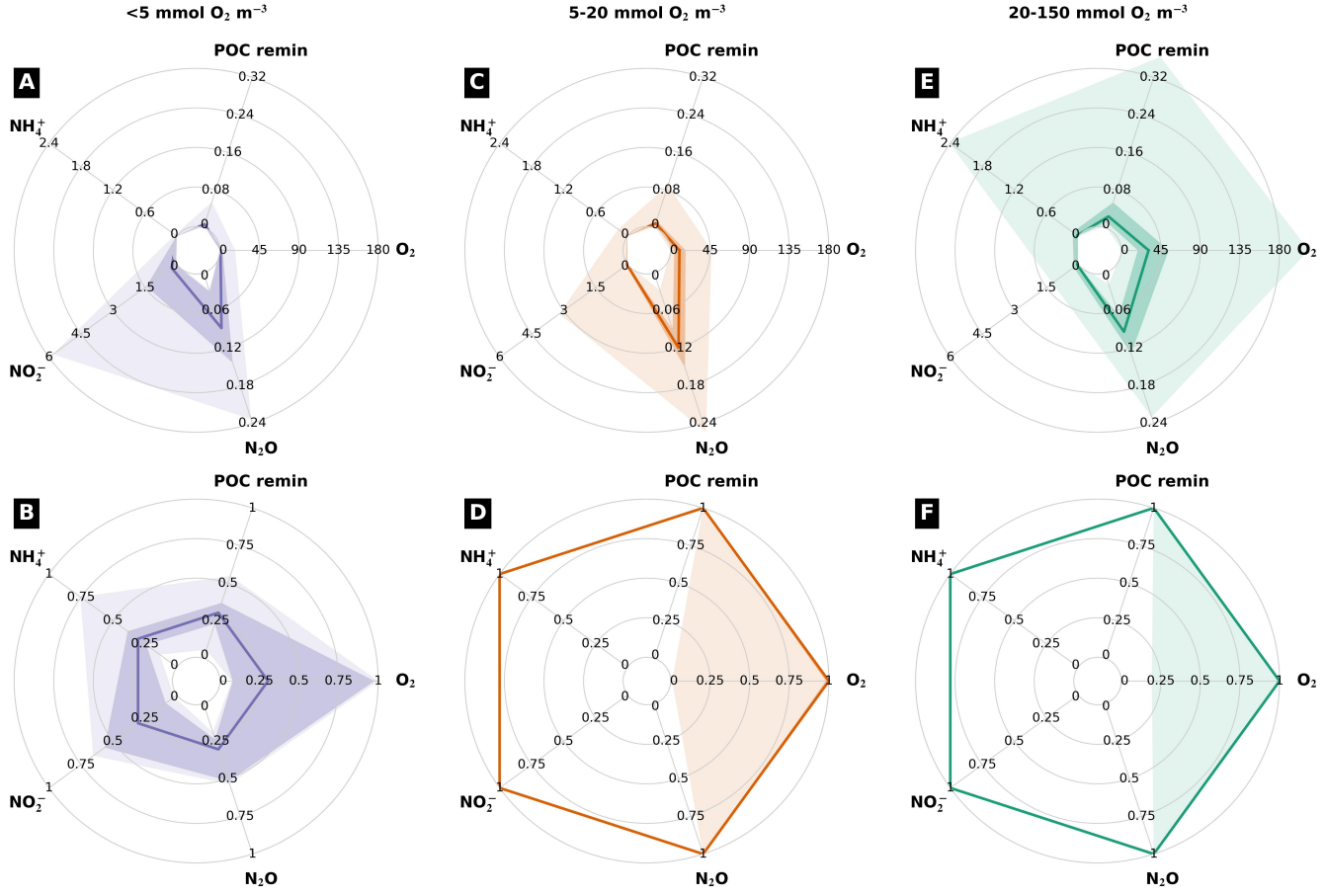


Figure 8. Spatiotemporal variability of the controlling variables (first row, A, C, & E) and its effect on the anammox to denitrification ratio (second row, B, D, & F). (A & B) show the results for the OMZ cores (less than 5 mmol O_2 m^{-3}), (C & D) the oxyclines (5 to 20 mmol O_2 m^{-3}), and (E & F) the OMZ edges (20 to 150 mmol O_2 m^{-3}). Percentiles are computed over space and time within each region. The effect on the ratio is computed by varying one controlling variable across its percentiles while holding all others at their regional median. Darker shading shows the 25th–75th percentile range and lighter shading the 10th–90th percentile range, for both the controlling variables and the resulting ratio. Ammonium ($[NH_4^+]$), nitrite ($[NO_2^-]$), and nitrous oxide ($[N_2O]$) are shown in units of mmol N m^{-3}, oxygen ($[O_2]$) in units of mmol O_2 m^{-3}, and particulate organic carbon (POC) remineralization in units of mmol C m^{-3} d^{-1}.

https://doi.org/10.5194/egusphere-2026-6541
Preprint. Discussion started: 29 October 2026
© Author(s) 2026. CC BY 4.0 License.

Our findings refine the hypothesis of Dalsgaard et al. (2012), who proposed that denitrification, unlike anammox, occurs in short, intense pulses triggered by pulses in organic matter export. They further hypothesized that, since such pulses are easily missed by discrete sampling, observations underestimate denitrification and thus overestimate the anammox to denitrification ratio. Our model supports the pulsed nature of denitrification, with transient rates exceeding 8000 μmol N m^{-3} d^{-1}, while 41-year mean rates reach at most ∼60 μmol N m^{-3} d^{-1}. The model also suggests that snapshots are likely to miss these pulses, partially explaining the mismatch between the observed and stoichiometrically expected ratios. However, these pulses are not determined by organic matter export alone: they occur only when high remineralization rates, fueled by organic matter export, coincide with non-limiting N_2O concentrations and anoxic conditions. Organic matter export is thus necessary but not sufficient, and oxygen is the primary control on these pulses.

In the following, we test whether the anammox to denitrification ratio covaries with net N_2O production and examine what drives the underlying oxygen variability on subseasonal and interannual timescales.

4.5 Covariation of the Anammox to Denitrification Ratio with Net Nitrous Oxide Production

In a representative snapshot of the anammox to denitrification ratio and net N_2O production at 200 m depth on 31 January 2004, a high anammox to denitrification ratio coincides with positive net N_2O production, while a low ratio coincides with net N_2O consumption (Fig. 9A & B). The ratio, however, does not scale with the magnitude of net N_2O production and therefore only indicates whether N_2O is produced or consumed. The magnitude of net N_2O production likely depends more strongly on remineralization rates and on the concentrations of NO_2^- and N_2O.

On subseasonal timescales, both the anammox to denitrification ratio and net N_2O production are strongly shaped by oxygen (Fig. 9C), which is consistent with our driver analysis (Fig. 8). Higher [O_2] allows anammox to outcompete denitrification, and N_2O production to exceed N_2O consumption, while lower [O_2] favors the opposite in both cases. Oxygen variability is primarily driven by mesoscale dynamics, especially by jets, filaments, and mesoscale eddies (Bettencourt et al., 2015; Margolskee et al., 2019; Köhn et al., 2022; Lee-Sánchez et al., 2026). In the ETNP, North Equatorial Undercurrent jets ventilate the region with oxygenated waters (Margolskee et al., 2019), driving oxygen intrusions such as the one at around 12°N. This intrusion raises [O_2] enough to temporarily shift N loss to being fully anammox-dominated and results in N_2O production, supporting the hypothesis of Babbin et al. (2015) that oxygen intrusions lead to N_2O production. Anticyclonic eddies originating from the Gulf of Tehuantepec, such as the one we identified at about 100°W, 14°N, deepen the oxycline and elevate [O_2], whereas cyclonic eddies, such as the one we identified at about 100°W, 10°N, shoal it and further lower [O_2] (Lee-Sánchez et al., 2026). Accordingly, the anticyclonic eddy shifts N loss toward anammox and produces N_2O, with the highest N_2O production occurring near its margin, which agrees with observations by Monreal et al. (2022). The cyclonic eddy, in contrast, increases the relative contribution of denitrification to N loss and drives N_2O consumption. Similar eddies have been reported in the ETSP, but with the opposite effect on oxygen: anticyclonic eddies are generally associated with low [O_2] and cyclonic eddies with high [O_2] (Stramma et al., 2013; Thomsen et al., 2016). The spatial patterns of the other controlling variables are shown in Fig. A6 for comparison.

https://doi.org/10.5194/egusphere-2026-6541
Preprint. Discussion started: 29 October 2026
© Author(s) 2026. CC BY 4.0 License.

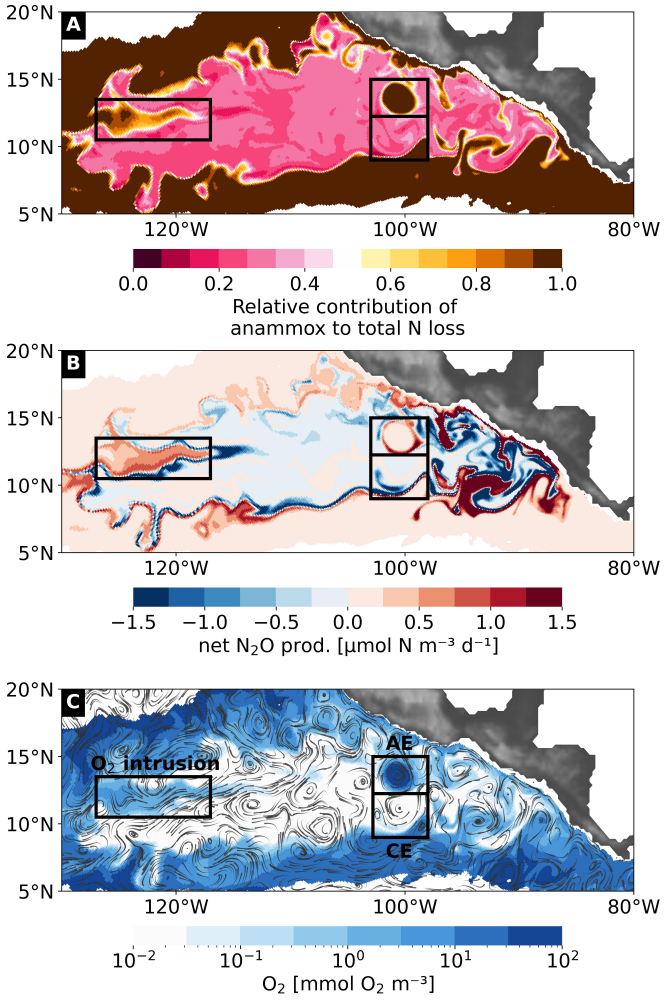


Figure 9. Spatial distribution of (A) the anammox to denitrification ratio (f_{ax}), (B) net nitrous oxide (N_2O) production, and (C) oxygen ($[O_2]$), with velocity streamlines overlain. Fields show a snapshot at 200 m on 31 January 2004 and are only shown for the Eastern Tropical North Pacific. The black boxes highlight an oxygen intrusion, an anticyclonic eddy (AE), and a cyclonic eddy (CE).

On interannual timescales, the anammox to denitrification ratio and net N_2O production are only partially coupled (Fig. 10). In the OMZ cores and oxyclines, both increase during El Niño and decrease during La Niña, driven by higher $[O_2]$ during El Niño due to a contraction of the OMZs and lower $[O_2]$ during La Niña due to their shoaling and expansion (Fig. A7A; Yang et al., 2017). At the OMZ edges, however, this relationship breaks down: while the anammox to denitrification ratio still increases during El Niño and decreases during La Niña, net N_2O production decreases during El Niño and increases during La Niña. The anammox to denitrification ratio is thus not a reliable predictor of ENSO-driven changes in net N_2O production. This edge-like response of net N_2O production also dominates at larger scales: integrated over the entire ETP down to 1000 m depth, net N_2O production decreases during El Niño and increases during La Niña (Härri et al., 2026a).

https://doi.org/10.5194/egusphere-2026-6541
Preprint. Discussion started: 29 October 2026
© Author(s) 2026. CC BY 4.0 License.

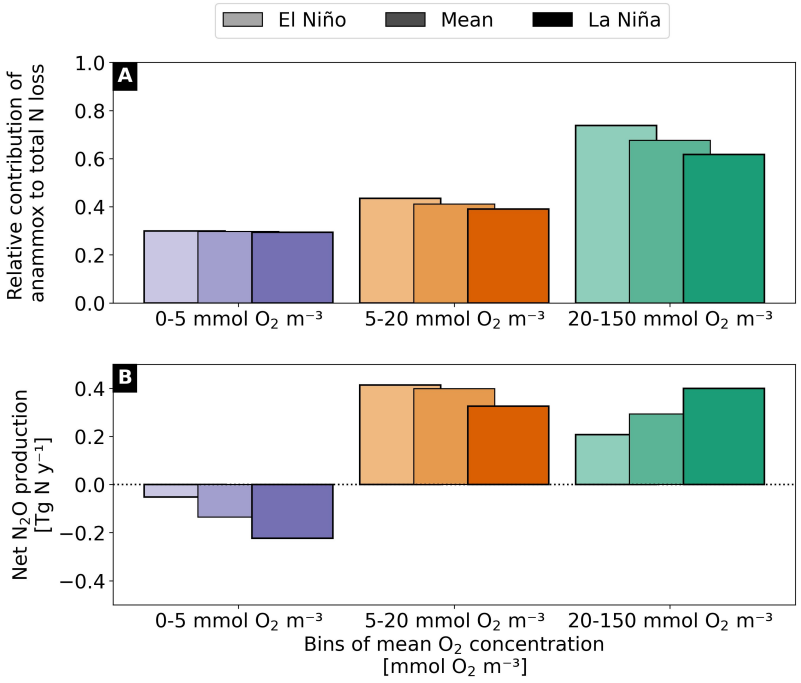


Figure 10. Impact of El Niño and La Niña on (A) the anammox to denitrification ratio (f_{ax}), and (B) net nitrous oxide (N_2O) production. The results are composited for 115 El Niño months, the 41-year mean, and 116 La Niña months, and shown separately for the OMZ cores, oxyclines, and OMZ edges.

Nonetheless, ENSO might illustrate how the ratio and net N_2O production diverge under future change. By 2100, the OMZ edges, where N loss is anammox-dominated, are projected to expand in volume, while the OMZ cores and oxyclines slightly contract (Busecke et al., 2022). These diverging fates would likely increase the relative contribution of anammox to total N loss, and are expected to result in more N_2O production at the OMZ edges and less N_2O consumption in the OMZ cores (Härri et al., 2026a). El Niño events are also projected to intensify under continued warming (Cai et al., 2023), which would further increase the relative contribution of anammox within each region of the OMZ. However, an intensification of El Niño is expected to decrease net N_2O production when integrated over the entire ETP (Härri et al., 2026a). Thus, while the future trajectory of the anammox to denitrification ratio appears clear, with both OMZ restructuring and El Niño intensification favoring anammox within each region of the OMZ, the future trajectory of net N_2O production remains uncertain, as the two drivers act in opposite directions.

5 Caveats and Limitations

A key limitation of this study is the scarcity of observations available to evaluate the modeled N loss pathways. Critically, existing measurements are biased toward regions and periods where anammox dominates N loss, which prevents us from

https://doi.org/10.5194/egusphere-2026-6541
Preprint. Discussion started: 29 October 2026
© Author(s) 2026. CC BY 4.0 License.

evaluating our central finding that denitrification drives the majority of N loss when integrated over the entire ETP. Targeted offshore observations, repeated over time, are therefore needed, particularly in the OMZ cores, where our model suggests that denitrification dominates N loss. Observations that resolve ETP-wide N loss dynamics are also needed to track how N loss responds as OMZs change in extent and structure (Busecke et al., 2022).

The oxygen inhibition constants of anammox and denitrification, which set how strongly oxygen controls the anammox to denitrification ratio, are a further source of uncertainty. In NitrOMZ, these constants were initially based on experimental estimates by Dalsgaard et al. (2014) and then tuned jointly with the other model parameters to reproduce observed profiles of nitrogen species and rates of the nitrogen cycle processes represented in the model (Bianchi et al., 2023). While the resulting $K_{den3}^{O_2}$ is of the same order of magnitude as the experimental estimate, $K_{ax}^{O_2}$ is considerably higher, making anammox in the model less sensitive to oxygen than suggested by these experiments. These experimental estimates carry considerable uncertainty, so that the contrast in oxygen sensitivity between the two pathways remains poorly constrained. A smaller contrast, as suggested by the experimental estimates, would make the transition from denitrification- to anammox-dominated N loss more gradual and would increase the influence of substrate supply and remineralization on the ratio and its variability. Adopting the experimental constants, however, would substantially reduce anammox rates, preventing the model from reproducing the observed profiles of anammox and denitrification rates, and, since all processes in NitrOMZ are interconnected, would also affect the other nitrogen cycle processes.

A shortcoming of our model is that it does not resolve three processes proposed to supply additional NH_4^+ and thereby increase the relative contribution of anammox to N loss: DNRA (Lam et al., 2009), NH_4^+ excretion by vertically migrating zooplankton (Bianchi et al., 2014), and NH_4^+ release from sediments (Kalvelage et al., 2013). DNRA is important in sediments but has only been observed sporadically in OMZs (Lam et al., 2009; Kalvelage et al., 2011; De Brabandere et al., 2014), and its role in the water column remains debated (Bianchi et al., 2023). Zooplankton excretion has been estimated to increase the fraction of anammox-driven N loss by about 0.1, depending strongly on the assumed fraction of active zooplankton transport (Bianchi et al., 2014). Even with such a shift, denitrification would still dominate N loss across the ETP, unlike the anammox dominance reported by observations. Sedimentary NH_4^+ release only affects the water column where the OMZs are in direct contact with the seafloor, which in the ETP is limited to a narrow band along the continental shelf. Including it would likely raise the modeled anammox share at the predominantly coastal sampling locations, bringing the model closer to the observations with little effect on the ETP-wide ratio. Overall, these missing NH_4^+ sources may shift the mean anammox to denitrification ratio toward anammox. Our findings on where the ratio varies, on which timescales, and what controls this variability are, however, unlikely to change qualitatively, since this variability arises primarily from oxygen fluctuations.

Our model also does not resolve the sinking and remineralization of individual particles, which have been hypothesized to create localized, particle-associated hotspots of denitrification-driven N loss (Bianchi et al., 2018; Tracey et al., 2023). Instead, our model represents remineralization as a process averaged over each grid cell, which may underestimate the role of organic matter pulses in triggering denitrification pulses, as proposed by Dalsgaard et al. (2012). This limitation might therefore lead our model to underestimate the relative contribution of denitrification to total N loss, particularly during such particle-associated events. The bias from missing NH_4^+ sources toward underestimating anammox and the bias from unresolved

https://doi.org/10.5194/egusphere-2026-6541
Preprint. Discussion started: 29 October 2026
© Author(s) 2026. CC BY 4.0 License.

particle-scale remineralization toward underestimating denitrification may partially offset one another. However, the extent to which they compensate for each other is unknown.

6 Conclusions

Here, we employ a recently developed nitrogen-cycling module to constrain total N loss in the ETP and to quantify the relative contributions of anammox and denitrification. Despite decades of effort, stoichiometric expectations and observations of the anammox to denitrification ratio have remained at odds. We show that this mismatch arises mainly from spatial sampling bias combined with a pronounced spatial pattern in the ratio itself, and to a lesser extent from temporal sampling bias. Our model reproduces the anammox-dominated N loss observed at sampling locations while simulating a ratio of 32:68 across the entire ETP — approaching the stoichiometric expectation of 29:71. Our results highlight that broader sampling coverage across the ETP is needed to capture the ETP-wide anammox to denitrification ratio.

To test whether the anammox to denitrification ratio at sampling sites is further biased toward anammox because denitrification occurs infrequently and in strong pulses, as hypothesized by Dalsgaard et al. (2012), we compared snapshots with long-term means and examined the timescales on which the ratio varies. At the sampling locations, the ratio is higher in the subsampled model output than in the long-term mean, indicating that snapshots are likely to miss denitrification pulses and thus partially explaining the mismatch between observed and stoichiometrically expected ratios. Such pulses are most likely to bias the ratio at the OMZ edges, whereas the ratio varies little in the OMZ cores and mainly on interannual timescales in the oxyclines. Refining the hypothesis of Dalsgaard et al. (2012), we find that these pulses are not set by organic matter export alone, but occur only when high remineralization rates coincide with anoxic conditions, so that most of the variability in the ratio is controlled by oxygen. Since oxygen also controls the balance between N_2O production and consumption, the anammox to denitrification ratio can indicate where N_2O is produced or consumed, though this relationship breaks down when integrated spatially.

Taken together, this work provides a detailed picture of the two principal N loss pathways in the ETP, covering their spatial distribution, relative magnitudes, temporal variability, and controlling variables — advances that carry broader significance given ongoing changes in the structure and volumes of the OMZ. By resolving the long-standing mismatch between the stoichiometrically expected and observed anammox to denitrification ratio, and by identifying the spatiotemporal controls on N loss partitioning, this work lays the groundwork for better anticipating how the ocean N cycle will respond to future environmental change. By 2100, the OMZ edges are projected to expand while the OMZ cores and oxyclines might slightly contract (Busecke et al., 2022), a redistribution that, based on our findings, might increase the relative contribution of anammox to total N loss, with associated increases in N_2O production at the OMZ edges and a reduced volume for N_2O consumption in the OMZ cores.

https://doi.org/10.5194/egusphere-2026-6541
Preprint. Discussion started: 29 October 2026
© Author(s) 2026. CC BY 4.0 License.



Data availability. The data underlying the results and figures are stored on the ETH Research Collection (Härri et al., 2026b): https://doi.org/10.3929/ethz-c-000806407.

Appendix A

A1 Model Parameterization

Table A1. Overview of the most important NitrOMZ parameters.

Parameter	Description	Units	Value
k_{remin}	Maximum aerobic remineralization rate	mmol C m^{-3} d^{-1}	0.08
k_{ao}	Maximum NH_4^+ oxidation rate	mmol N m^{-3} d^{-1}	0.05
k_{no}	Maximum NO_2^- oxidation rate	mmol N m^{-3} d^{-1}	0.05
k_{den1}	Maximum NO_3^- reduction rate	mmol C m^{-3} d^{-1}	0.016
k_{den2}	Maximum NO_2^- reduction rate	mmol C m^{-3} d^{-1}	0.008
k_{den3}	Maximum N_2O reduction rate	mmol C m^{-3} d^{-1}	0.0496
k_{ax}	Maximum anammox rate	mmol N_2 m^{-3} d^{-1}	0.441
$K_{remin}^{O_2}$	O_2 half-saturation constant for aerobic remineralization	mmol O_2 m^{-3}	1
$K_{ao}^{NH_4^+}$	NH_4^+ half-saturation constant for NH_4^+ oxidation	mmol N m^{-3}	0.305
$K_{ao}^{O_2}$	O_2 half-saturation constant for NH_4^+ oxidation	mmol O_2 m^{-3}	0.333
$K_{no}^{NO_2^-}$	NO_2^- half-saturation constant for NO_2^- oxidation	mmol N m^{-3}	0.509
$K_{no}^{O_2}$	O_2 half-saturation constant for NO_2^- oxidation	mmol O_2 m^{-3}	0.778
$K_{den1}^{NO_3^-}$	NO_3^- half-saturation constant for NO_3^- reduction	mmol N m^{-3}	1
$K_{den2}^{NO_2^-}$	NO_2^- half-saturation constant for NO_2^- reduction	mmol N m^{-3}	0.01
$K_{den3}^{N_2O}$	N_2O half-saturation constant for N_2O reduction	mmol N_2 m^{-3}	0.159
$K_{ax}^{NH_4^+}$	NH_4^+ half-saturation constant for anammox	mmol N m^{-3}	1
$K_{ax}^{NO_2^-}$	NO_2^- half-saturation constant for anammox	mmol N m^{-3}	1
$K_{den1}^{O_2}$	O_2 exponential inhibition for NO_3^- reduction	mmol O_2 m^{-3}	6
$K_{den2}^{O_2}$	O_2 exponential inhibition for NO_2^- reduction	mmol O_2 m^{-3}	2.3
$K_{den3}^{O_2}$	O_2 exponential inhibition for N_2O reduction	mmol O_2 m^{-3}	0.506
$K_{ax}^{O_2}$	O_2 exponential inhibition for anammox	mmol O_2 m^{-3}	6

https://doi.org/10.5194/egusphere-2026-6541
Preprint. Discussion started: 29 October 2026
© Author(s) 2026. CC BY 4.0 License.

A2 Additional Figures Supporting Methods

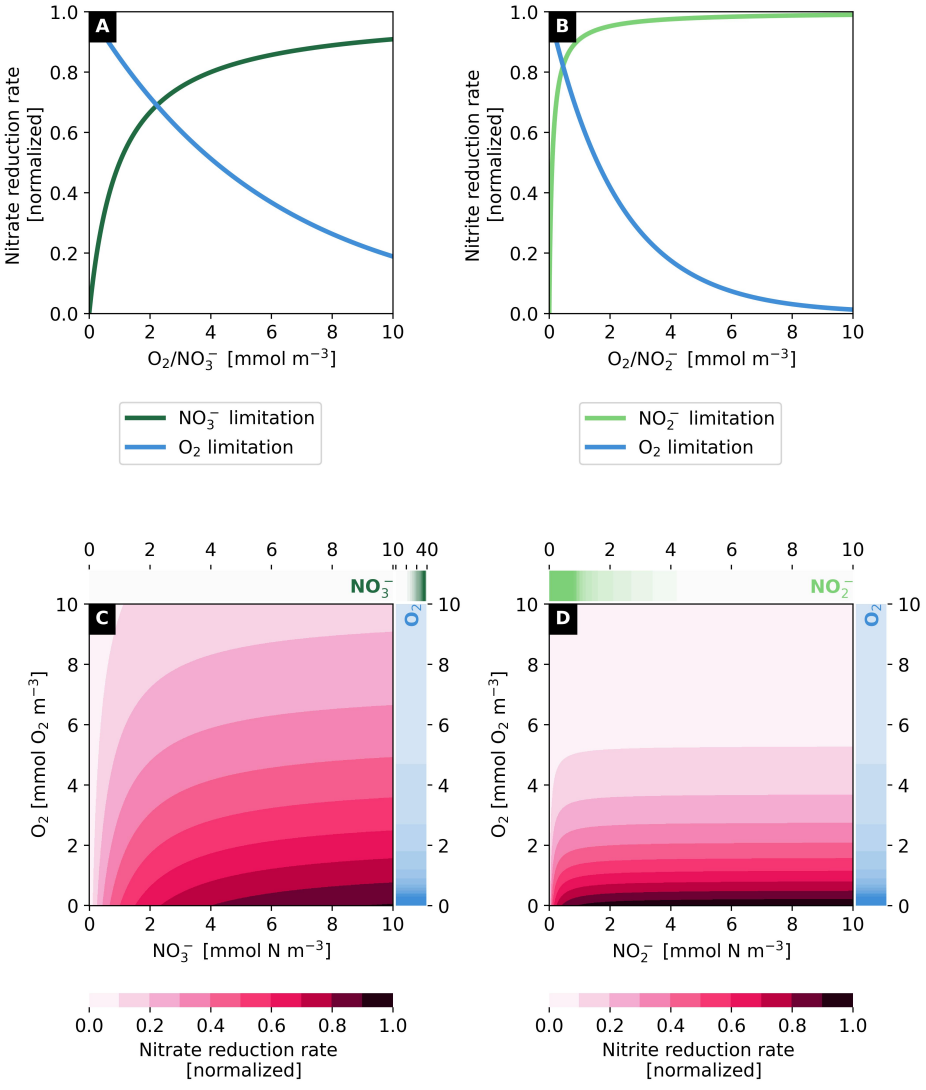


Figure A1. Parameterization of the nitrate (NO_3^-) and nitrite (NO_2^-) reduction rates in NitrOMZ. (A & B) Nitrate and nitrite reduction rates as a function of oxygen (O_2) and the respective substrate (NO_3^-, NO_2^-). (C & D) Contour plots of the NO_3^- and NO_2^- reduction rates as a function of O_2 and the respective substrate. The colorbars indicate the concentrations at which O_2, NO_3^-, and NO_2^- occur in the study region where [O_2] is below 10 mmol O_2 m^{-3} in the 41-year mean, with darker colors indicating higher occurrence.

https://doi.org/10.5194/egusphere-2026-6541
Preprint. Discussion started: 29 October 2026
© Author(s) 2026. CC BY 4.0 License.

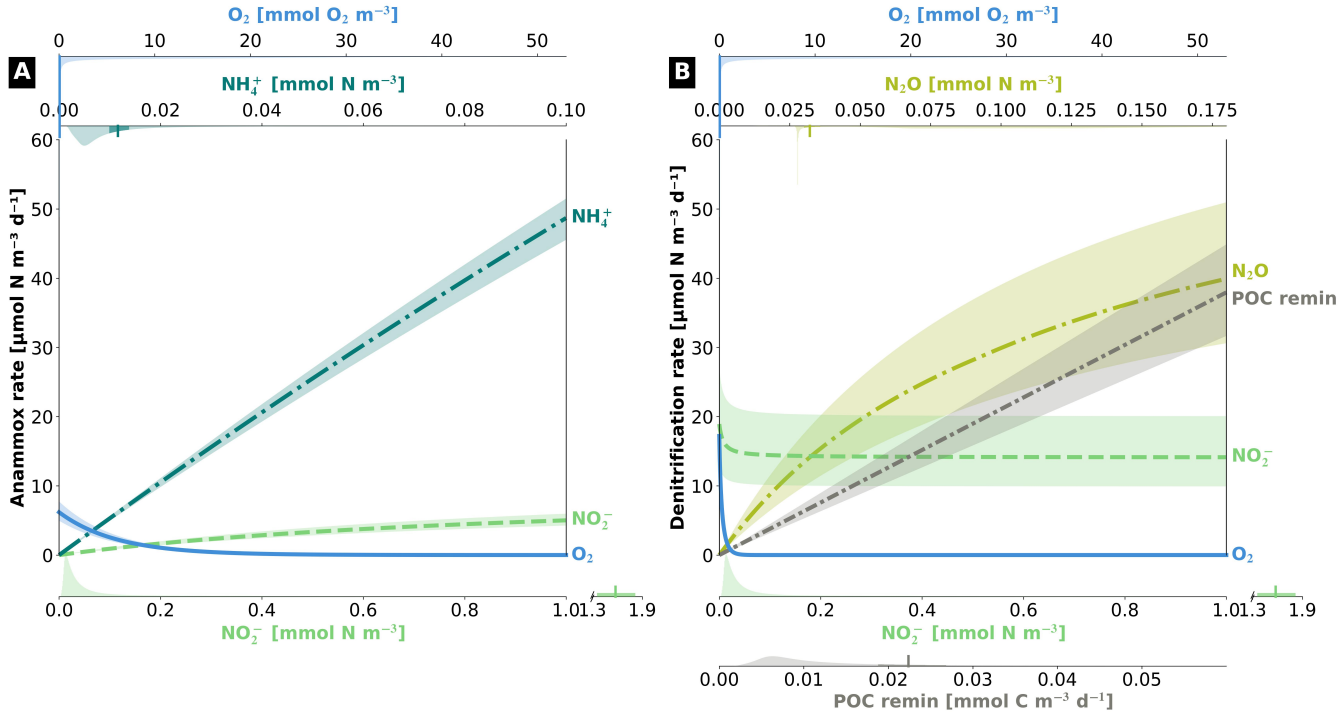


Figure A2. Idealized analysis of the dependence of the (A) anammox and (B) denitrification rates on the six controlling variables. Each line shows, for one variable at a time, how the rate changes as that variable varies. The other variables were fixed at five reference values spanning their nitrogen-loss-weighted 45th–55th percentiles, including the median, and the response was computed for every combination. The thick line gives the median response and the shading the minimum-to-maximum range across all combinations. Controlling variables are shown from 0 to their 90th percentile, taking into account only regions where anammox and denitrification are present in the 41-year mean. The histogram on each axis shows that variable's distribution across these regions. The darker histogram bars and vertical line mark the nitrogen-loss-weighted 45th–55th percentile range and median of that variable. Due to computational constraints, only every 5th day and every 3rd grid cell was considered.

https://doi.org/10.5194/egusphere-2026-6541
Preprint. Discussion started: 29 October 2026
© Author(s) 2026. CC BY 4.0 License.

A3 Additional Figures Supporting Results

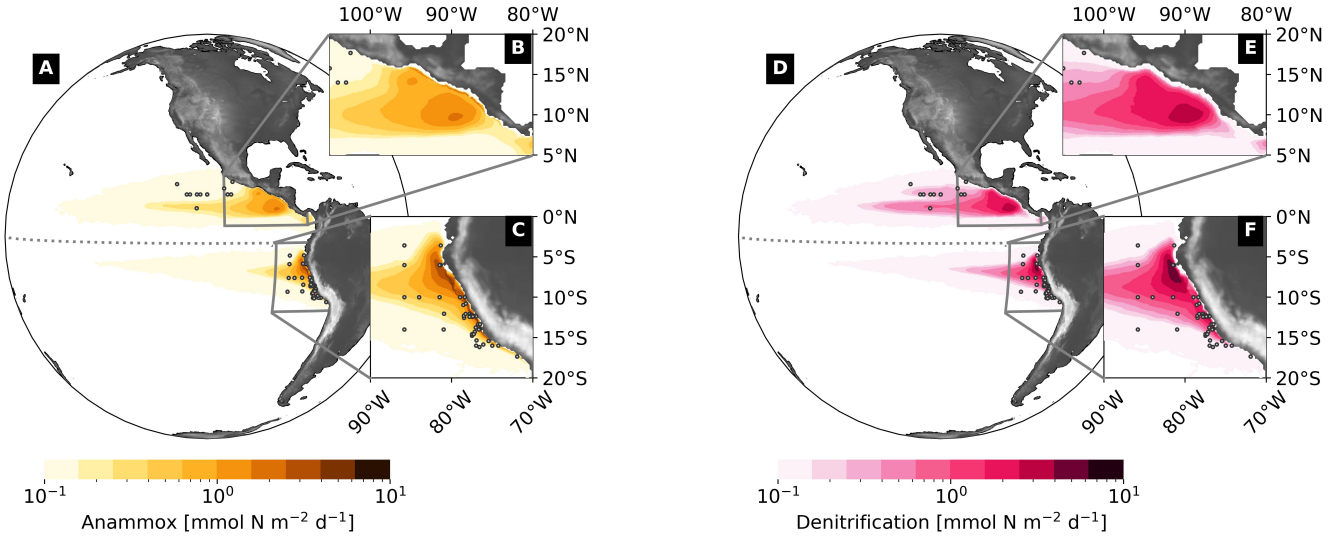


Figure A3. Anammox and denitrification rates integrated over the top 300 m and averaged over 41 years. (A) Depth-integrated anammox rates, with circles indicating sampling locations; (B) and (C) show zooms of the northern and southern Eastern Tropical Pacific, respectively. (D–F) Same as (A–C), but for denitrification rates.

https://doi.org/10.5194/egusphere-2026-6541
Preprint. Discussion started: 29 October 2026
© Author(s) 2026. CC BY 4.0 License.

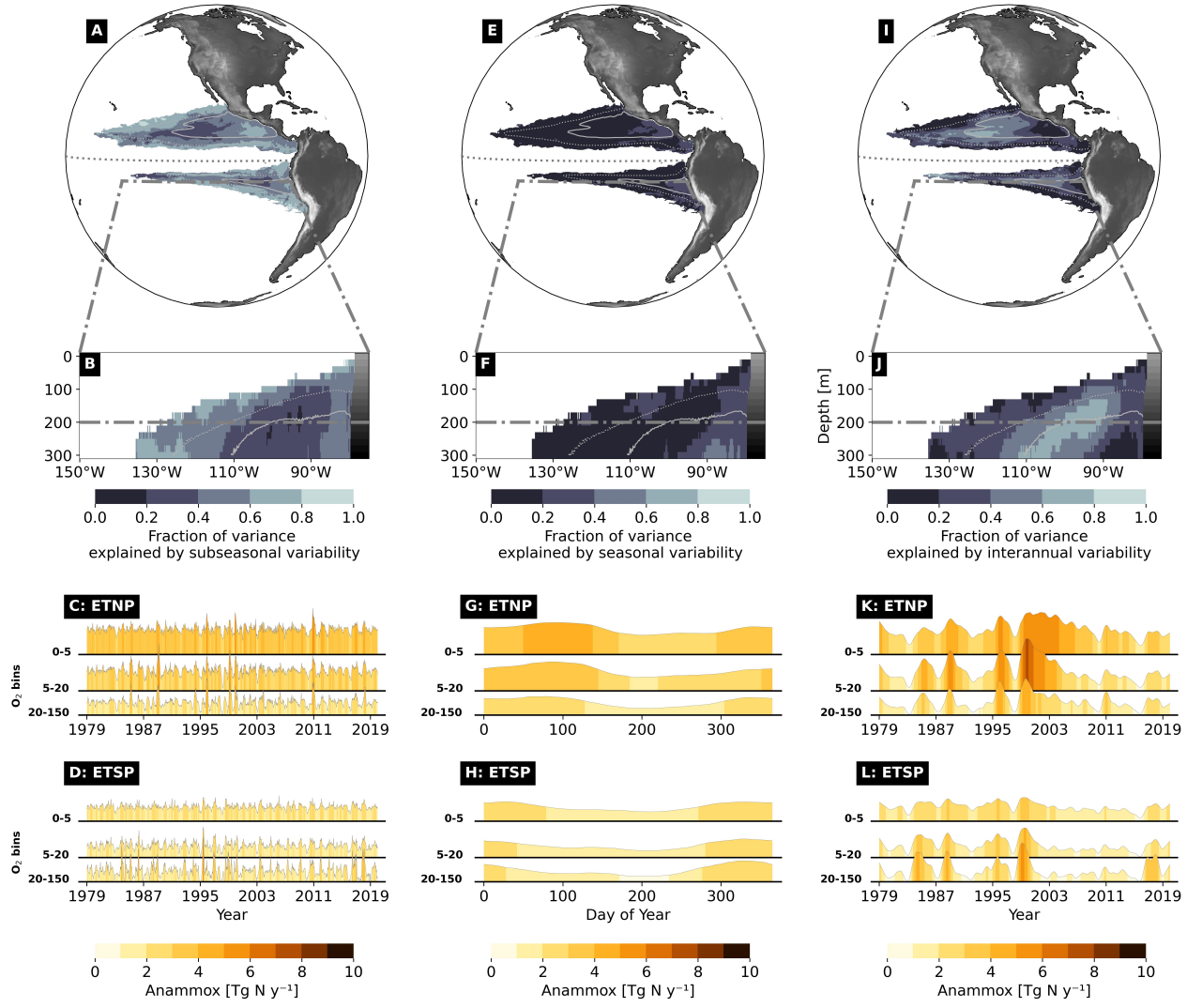


Figure A4. Subseasonal, seasonal, and interannual variability in the anammox rate. Panels (A) and (B) show the fraction of variability explained by subseasonal variability at 200 m and along the 8°S transect, respectively. Panels (C) and (D) show subseasonal variability in the volume-integrated anammox rates in the OMZ cores, oxyclines, and OMZ edges of the ETNP and ETSP, respectively. Panels (E–H) and (I–L) show the same decomposition for seasonal and interannual variability, respectively. The solid and dotted contours depict the 5 and 20 mmol O_2 m^{-3} thresholds in the 41-year mean, respectively, delineating the boundaries between the OMZ cores, oxyclines, and OMZ edges.

https://doi.org/10.5194/egusphere-2026-6541
Preprint. Discussion started: 29 October 2026
© Author(s) 2026. CC BY 4.0 License.

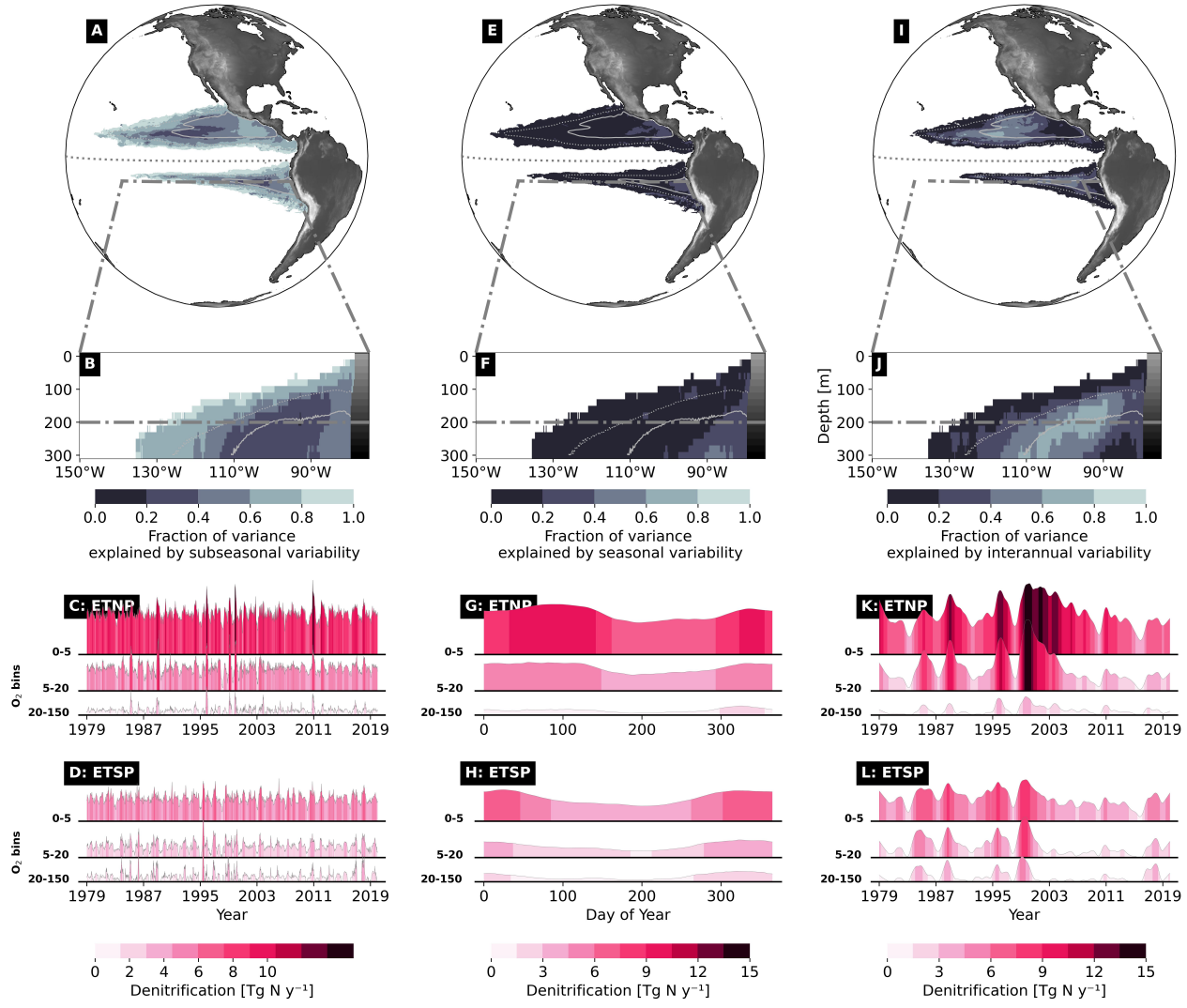


Figure A5. Subseasonal, seasonal, and interannual variability in the denitrification rate. Panels (A) and (B) show the fraction of variability explained by subseasonal variability at 200 m and along the 8°S transect, respectively. Panels (C) and (D) show subseasonal variability in the volume-integrated denitrification rates in the OMZ cores, oxyclines, and OMZ edges of the ETNP and ETSP, respectively. Panels (E–H) and (I–L) show the same decomposition for seasonal and interannual variability, respectively. The solid and dotted contours depict the 5 and 20 mmol O_2 m^{-3} thresholds in the 41-year mean, respectively, delineating the boundaries between the OMZ cores, oxyclines, and OMZ edges.

https://doi.org/10.5194/egusphere-2026-6541
Preprint. Discussion started: 29 October 2026
© Author(s) 2026. CC BY 4.0 License.

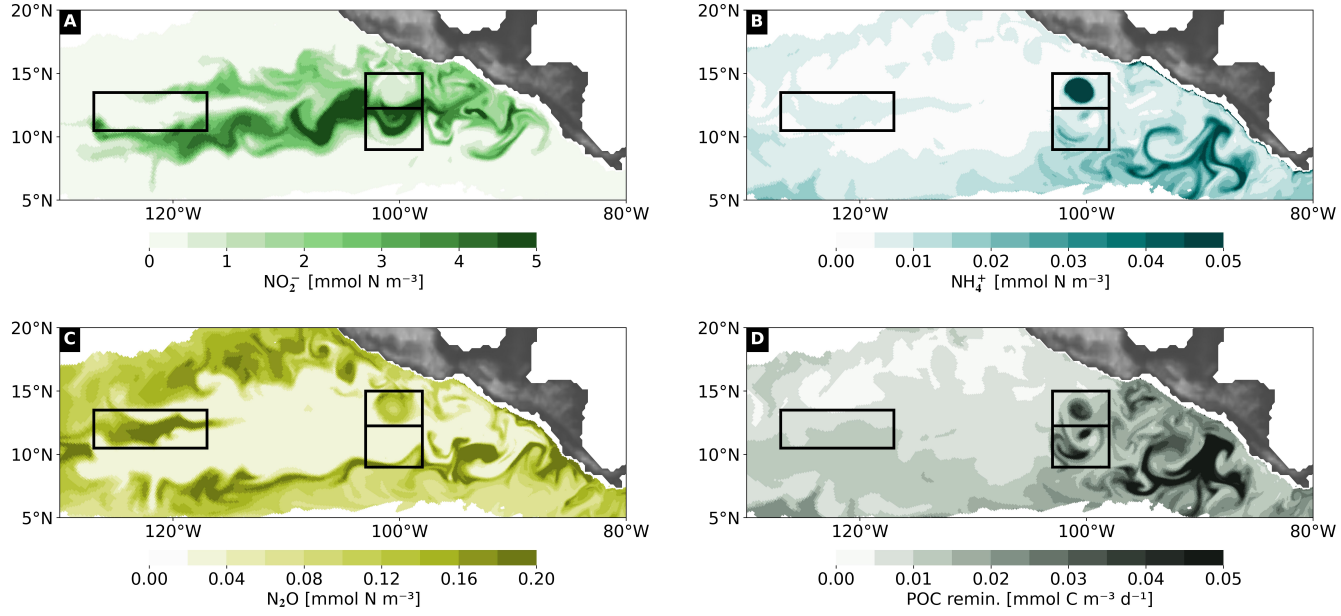


Figure A6. Spatial distribution of the (A) nitrite ([NO_2^-]), (B) ammonium ([NH_4^+]), (C) nitrous oxide ([N_2O]), and (D) particulate organic carbon (POC) remineralization rate. Fields show a snapshot at 200 m on 31 January 2004 and are only shown for the Eastern Tropical North Pacific. The black boxes highlight an oxygen intrusion, an anticyclonic eddy (AE), and a cyclonic eddy (CE).

https://doi.org/10.5194/egusphere-2026-6541
Preprint. Discussion started: 29 October 2026
© Author(s) 2026. CC BY 4.0 License.

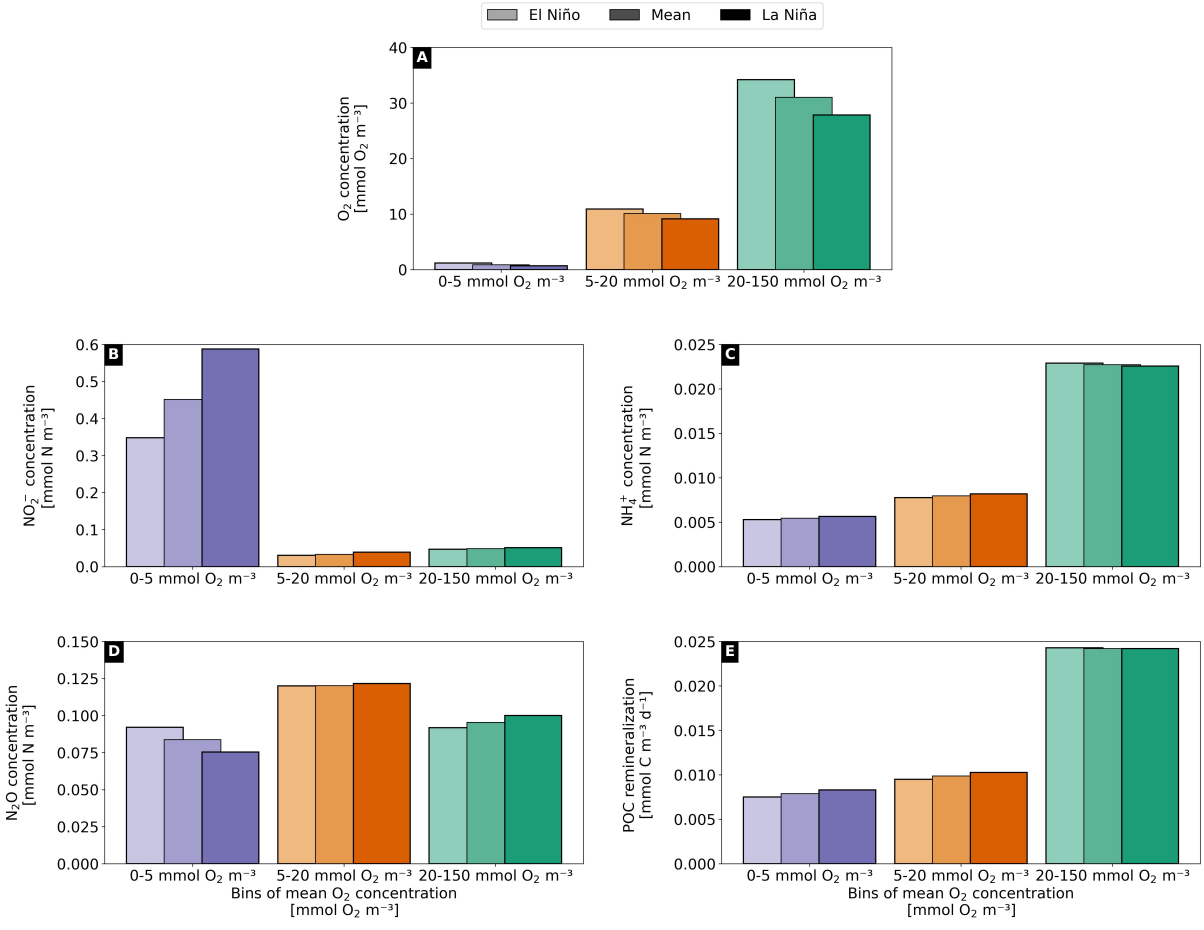


Figure A7. Impact of El Niño and La Niña on (A) oxygen ($[O_2]$), (B) nitrite ($[NO_2^-]$), (C) ammonium ($[NH_4^+]$), (D) nitrous oxide ($[N_2O]$), and (E) particulate organic carbon (POC) remineralization rate. The results are composited for 115 El Niño months, the 41-year mean, and 116 La Niña months, and shown separately for the OMZ cores, oxyclines, and OMZ edges.

https://doi.org/10.5194/egusphere-2026-6541
Preprint. Discussion started: 29 October 2026
© Author(s) 2026. CC BY 4.0 License.

Author contributions. J.H. led the analysis and the writing of the paper. M.V. contributed to the interpretation of results and editing of the manuscript. N.G. acquired funding, oversaw the project progress, and contributed to the interpretation of results and editing of the manuscript.

Competing interests. The authors declare there are no conflicts of interest for this manuscript.

Acknowledgements. This study received financial support from ETH Zürich. We would like to thank Daniel McCoy for the insightful discussion on this manuscript and Daniele Bianchi for sharing the NitrOMZ code with us. The writing process of this manuscript was supported by the artificial intelligence tools *Writefull* and *Claude*.

https://doi.org/10.5194/egusphere-2026-6541
Preprint. Discussion started: 29 October 2026
© Author(s) 2026. CC BY 4.0 License.

References

Babbin, A. R., Keil, R. G., Devol, A. H., and Ward, B. B.: Organic Matter Stoichiometry, Flux, and Oxygen Control Nitrogen Loss in the Ocean, Science, 344, 406–408, https://doi.org/10.1126/science.1248364, 2014.

Babbin, A. R., Bianchi, D., Jayakumar, A., and Ward, B. B.: Rapid nitrous oxide cycling in the suboxic ocean, Science, 348, 1127–1129, https://doi.org/10.1126/science.aaa8380, 2015.

Babbin, A. R., Peters, B. D., Mordy, C. W., Widner, B., Casciotti, K. L., and Ward, B. B.: Multiple metabolisms constrain the anaerobic nitrite budget in the Eastern Tropical South Pacific, Global Biogeochemical Cycles, 31, 258–271, https://doi.org/10.1002/2016GB005407, 2017.

Bettencourt, J. H., López, C., Hernández-García, E., Montes, I., Sudre, J., Dewitte, B., Paulmier, A., and Garçon, V.: Boundaries of the Peruvian oxygen minimum zone shaped by coherent mesoscale dynamics, Nature Geoscience, 8, 937–940, https://doi.org/10.1038/ngeo2570, 2015.

Bianchi, D., Dunne, J. P., Sarmiento, J. L., and Galbraith, E. D.: Data-based estimates of suboxia, denitrification, and N2O production in the ocean and their sensitivities to dissolved O2, Global Biogeochemical Cycles, 26, 1–13, https://doi.org/10.1029/2011GB004209, 2012.

Bianchi, D., Babbin, A. R., and Galbraith, E. D.: Enhancement of anammox by the excretion of diel vertical migrators, Proceedings of the National Academy of Sciences, 111, 15 653–15 658, https://doi.org/10.1073/pnas.1410790111, 2014.

Bianchi, D., Weber, T. S., Kiko, R., and Deutsch, C.: Global niche of marine anaerobic metabolisms expanded by particle microenvironments, Nature Geoscience, 11, 263–268, https://doi.org/10.1038/s41561-018-0081-0, 2018.

Bianchi, D., McCoy, D., and Yang, S.: Formulation, optimization, and sensitivity of NitrOMZv1.0, a biogeochemical model of the nitrogen cycle in oceanic oxygen minimum zones, Geoscientific Model Development, 16, 3581–3609, https://doi.org/10.5194/gmd-16-3581-2023, 2023.

Bristow, L. A., Dalsgaard, T., Tiano, L., Mills, D. B., Bertagnolli, A. D., Wright, J. J., Hallam, S. J., Ulloa, O., Canfield, D. E., Revsbech, N. P., and Thamdrup, B.: Ammonium and nitrite oxidation at nanomolar oxygen concentrations in oxygen minimum zone waters, Proceedings of the National Academy of Sciences, 113, 10 601–10 606, https://doi.org/10.1073/pnas.1600359113, 2016.

Busecke, J. J., Resplandy, L., Ditkovsky, S. J., and John, J. G.: Diverging Fates of the Pacific Ocean Oxygen Minimum Zone and Its Core in a Warming World, AGU Advances, 3, https://doi.org/10.1029/2021AV000470, 2022.

Cai, W., Ng, B., Geng, T., Jia, F., Wu, L., Wang, G., Liu, Y., Gan, B., Yang, K., Santoso, A., Lin, X., Li, Z., Liu, Y., Yang, Y., Jin, F.-F., Collins, M., and McPhaden, M. J.: Anthropogenic impacts on twentieth-century ENSO variability changes, Nature Reviews Earth & Environment, 4, 407–418, https://doi.org/10.1038/s43017-023-00427-8, 2023.

Cinay, T., Dumit, D., Woosley, R. J., Boles, E. L., Kwiecinski, J. V., Mullen, S., Tamasi, T. J., Wolf, M. J., Kelly, C. L., Travis, N. M., Casciotti, K. L., and Babbin, A. R.: Coincident Biogenic Nitrite and pH Maxima Arise in the Upper Anoxic Layer in the Eastern Tropical North Pacific, Global Biogeochemical Cycles, 36, https://doi.org/10.1029/2022GB007470, 2022.

Dalsgaard, T., Thamdrup, B., Farías, L., and Revsbech, N. P.: Anammox and denitrification in the oxygen minimum zone of the eastern South Pacific, Limnology and Oceanography, 57, 1331–1346, https://doi.org/10.4319/lo.2012.57.5.1331, 2012.

Dalsgaard, T., Stewart, F. J., Thamdrup, B., De Brabandere, L., Revsbech, N. P., Ulloa, O., Canfield, D. E., and DeLong, E. F.: Oxygen at Nanomolar Levels Reversibly Suppresses Process Rates and Gene Expression in Anammox and Denitrification in the Oxygen Minimum Zone off Northern Chile, mBio, 5, https://doi.org/10.1128/mBio.01966-14, 2014.

https://doi.org/10.5194/egusphere-2026-6541
Preprint. Discussion started: 29 October 2026
© Author(s) 2026. CC BY 4.0 License.



De Brabandere, L., Canfield, D. E., Dalsgaard, T., Friederich, G. E., Revsbech, N. P., Ulloa, O., and Thamdrup, B.: Vertical partitioning of nitrogen-loss processes across the oxic-anoxic interface of an oceanic oxygen minimum zone, Environmental Microbiology, 16, 3041–3054, https://doi.org/10.1111/1462-2920.12255, 2014.

Deutsch, C., Gruber, N., Key, R. M., Sarmiento, J. L., and Ganachaud, A.: Denitrification and N2 fixation in the Pacific Ocean, Global Biogeochemical Cycles, 15, 483–506, https://doi.org/10.1029/2000GB001291, 2001.

Devol, A. H.: Denitrification Including Anammox, in: Nitrogen in the Marine Environment, pp. 263–301, Elsevier, https://doi.org/10.1016/B978-0-12-372522-6.00006-2, 2008.

DeVries, T., Deutsch, C., Rafter, P. A., and Primeau, F.: Marine denitrification rates determined from a global 3-D inverse model, Biogeosciences, 10, 2481–2496, https://doi.org/10.5194/bg-10-2481-2013, 2013.

Dussin, R., Barnier, B., Brodeau, L., and Molines, J. M.: The making of the Drakkar forcing set DFS5 , Tech. rep., LGGE, https://www.drakkar-ocean.eu/publications/reports, 2016.

Fadum, J., Sun, X., and Zakem, E.: Redox-constrained microbial ecology dictates nitrogen loss versus retention, ISME Communications, 5, https://doi.org/10.1093/ismeco/ycaf219, 2025.

Falkowski, P. G.: Evolution of the nitrogen cycle and its influence on the biological sequestration of CO2 in the ocean, Nature, 387, 272–275, https://doi.org/10.1038/387272a0, 1997.

Fowler, D., Coyle, M., Skiba, U., Sutton, M. A., Cape, J. N., Reis, S., Sheppard, L. J., Jenkins, A., Grizzetti, B., Galloway, J. N., Vitousek, P., Leach, A., Bouwman, A. F., Butterbach-Bahl, K., Dentener, F., Stevenson, D., Amann, M., and Voss, M.: The global nitrogen cycle in the twenty-first century, Philosophical Transactions of the Royal Society B: Biological Sciences, 368, 20130164, https://doi.org/10.1098/rstb.2013.0164, 2013.

Frischknecht, M., Münnich, M., and Gruber, N.: Origin, Transformation, and Fate: The Three-Dimensional Biological Pump in the California Current System, Journal of Geophysical Research: Oceans, 123, 7939–7962, https://doi.org/10.1029/2018JC013934, 2018.

Ganesh, S., Parris, D. J., DeLong, E. F., and Stewart, F. J.: Metagenomic analysis of size-fractionated picoplankton in a marine oxygen minimum zone, The ISME Journal, 8, 187–211, https://doi.org/10.1038/ismej.2013.144, 2014.

Garcia-Robledo, E., Paulmier, A., Borisov, S. M., and Revsbech, N. P.: Sampling in low oxygen aquatic environments: The deviation from anoxic conditions, Limnology and Oceanography: Methods, 19, 733–740, https://doi.org/10.1002/lom3.10457, 2021.

Gruber, N.: The Marine Nitrogen Cycle: Overview and Challenges, in: Nitrogen in the Marine Environment, chap. 1, pp. 1–50, Elsevier, https://doi.org/10.1016/B978-0-12-372522-6.00001-3, 2008.

Hamersley, M. R., Lavik, G., Woebken, D., Rattray, J. E., Lam, P., Hopmans, E. C., Damsté, J. S. S., Krüger, S., Graco, M., Gutiérrez, D., and Kuypers, M. M. M.: Anaerobic ammonium oxidation in the Peruvian oxygen minimum zone, Limnology and Oceanography, 52, 923–933, https://doi.org/10.4319/lo.2007.52.3.0923, 2007.

Härri, J., McCoy, D., Vogt, M., Bianchi, D., and Gruber, N.: Impact of ENSO on Nitrous Oxide Emissions in the Eastern Tropical Pacific, Global Biogeochemical Cycles, 40, https://doi.org/10.1029/2025GB008739, 2026a.

Härri, J., Vogt, M., and Gruber, N.: The Anammox to Denitrification Ratio and its Environmental Controls in the Eastern Tropical Pacific [Dataset], 2026b.

Hersbach, H., Bell, B., Berrisford, P., Hirahara, S., Horányi, A., Muñoz-Sabater, J., Nicolas, J., Peubey, C., Radu, R., Schepers, D., Simmons, A., Soci, C., Abdalla, S., Abellan, X., Balsamo, G., Bechtold, P., Biavati, G., Bidlot, J., Bonavita, M., Chiara, G., Dahlgren, P., Dee, D., Diamantakis, M., Dragani, R., Flemming, J., Forbes, R., Fuentes, M., Geer, A., Haimberger, L., Healy, S., Hogan, R. J., Hólm, E., Janisková, M., Keeley, S., Laloyaux, P., Lopez, P., Lupu, C., Radnoti, G., Rosnay, P., Rozum, I., Vamborg, F., Villaume, S., and Thépaut,

https://doi.org/10.5194/egusphere-2026-6541
Preprint. Discussion started: 29 October 2026
© Author(s) 2026. CC BY 4.0 License.

J.: The ERA5 global reanalysis, Quarterly Journal of the Royal Meteorological Society, 146, 1999–2049, https://doi.org/10.1002/qj.3803, 2020.

Ji, Q., Babbin, A. R., Peng, X., Bowen, J. L., and Ward, B. B.: Nitrogen substrate–dependent nitrous oxide cycling in salt marsh sediments, Journal of Marine Research, 73, 71–92, https://doi.org/10.1357/002224015815848820, 2015.

Ji, Q., Buitenhuis, E., Suntharalingam, P., Sarmiento, J. L., and Ward, B. B.: Global Nitrous Oxide Production Determined by Oxygen Sensitivity of Nitrification and Denitrification, Global Biogeochemical Cycles, 32, 1790–1802, https://doi.org/10.1029/2018GB005887, 2018.

Kalvelage, T., Jensen, M. M., Contreras, S., Revsbech, N. P., Lam, P., Günter, M., LaRoche, J., Lavik, G., and Kuypers, M. M. M.: Oxygen Sensitivity of Anammox and Coupled N-Cycle Processes in Oxygen Minimum Zones, PLoS ONE, 6, e29 299, https://doi.org/10.1371/journal.pone.0029299, 2011.

Kalvelage, T., Lavik, G., Lam, P., Contreras, S., Arteaga, L., Löscher, C. R., Oschlies, A., Paulmier, A., Stramma, L., and Kuypers, M. M. M.: Nitrogen cycling driven by organic matter export in the South Pacific oxygen minimum zone, Nature Geoscience, 6, 228–234, https://doi.org/10.1038/ngeo1739, 2013.

Karthäuser, C., Ahmerkamp, S., Marchant, H. K., Bristow, L. A., Hauss, H., Iversen, M. H., Kiko, R., Maerz, J., Lavik, G., and Kuypers, M. M. M.: Small sinking particles control anammox rates in the Peruvian oxygen minimum zone, Nature Communications, 12, 3235, https://doi.org/10.1038/s41467-021-23340-4, 2021.

Koeve, W. and Kähler, P.: Heterotrophic denitrification vs. autotrophic anammox – quantifying collateral effects on the oceanic carbon cycle, Biogeosciences, 7, 2327–2337, https://doi.org/10.5194/bg-7-2327-2010, 2010.

Köhn, E. E., Münnich, M., Vogt, M., Desmet, F., and Gruber, N.: Strong Habitat Compression by Extreme Shoaling Events of Hypoxic Waters in the Eastern Pacific, Journal of Geophysical Research: Oceans, 127, https://doi.org/10.1029/2022JC018429, 2022.

Körner, H. and Zumft, W. G.: Expression of denitrification enzymes in response to the dissolved oxygen level and respiratory substrate in continuous culture of Pseudomonas stutzeri, Applied and Environmental Microbiology, 55, 1670–1676, https://doi.org/10.1128/aem.55.7.1670-1676.1989, 1989.

Kuypers, M. M. M., Marchant, H. K., and Kartal, B.: The microbial nitrogen-cycling network, Nature Reviews Microbiology, 16, 263–276, https://doi.org/10.1038/nrmicro.2018.9, 2018.

Lam, P., Lavik, G., Jensen, M. M., van de Vossenberg, J., Schmid, M., Woebken, D., Gutiérrez, D., Amann, R., Jetten, M. S. M., and Kuypers, M. M. M.: Revising the nitrogen cycle in the Peruvian oxygen minimum zone, Proceedings of the National Academy of Sciences, 106, 4752–4757, https://doi.org/10.1073/pnas.0812444106, 2009.

Lee-Sánchez, E., Sánchez-Velasco, L., Gutiérrez-Moreno, D. C., and Velásquez-Aristizábal, J. A.: Biogeochemical Response to Mesoscale Eddies and Tehuano Wind Events in the Oxygen Minimum Zone off the Gulf of Tehuantepec, Journal of Geophysical Research: Oceans, 131, https://doi.org/10.1029/2025JC023015, 2026.

Margolskee, A., Frenzel, H., Emerson, S., and Deutsch, C.: Ventilation Pathways for the North Pacific Oxygen Deficient Zone, Global Biogeochemical Cycles, 33, 875–890, https://doi.org/10.1029/2018GB006149, 2019.

McCoy, D., Damien, P., Clements, D., Yang, S., and Bianchi, D.: Pathways of Nitrous Oxide Production in the Eastern Tropical South Pacific Oxygen Minimum Zone, Global Biogeochemical Cycles, 37, https://doi.org/10.1029/2022GB007670, 2023.

Mogollón, R. and Calil, P. H.: On the effects of ENSO on ocean biogeochemistry in the Northern Humboldt Current System (NHCS): A modeling study, Journal of Marine Systems, 172, 137–159, https://doi.org/10.1016/j.jmarsys.2017.03.011, 2017.

https://doi.org/10.5194/egusphere-2026-6541
Preprint. Discussion started: 29 October 2026
© Author(s) 2026. CC BY 4.0 License.

Monreal, P. J., Kelly, C. L., Travis, N. M., and Casciotti, K. L.: Identifying the Sources and Drivers of Nitrous Oxide Accumulation in the Eddy-Influenced Eastern Tropical North Pacific Oxygen-Deficient Zone, Global Biogeochemical Cycles, 36, https://doi.org/10.1029/2022GB007310, 2022.

Moore, C. M., Mills, M. M., Arrigo, K. R., Berman-Frank, I., Bopp, L., Boyd, P. W., Galbraith, E. D., Geider, R. J., Guieu, C., Jaccard, S. L., Jickells, T. D., La Roche, J., Lenton, T. M., Mahowald, N. M., Marañón, E., Marinov, I., Moore, J. K., Nakatsuka, T., Oschlies, A., Saito, M. A., Thingstad, T. F., Tsuda, A., and Ulloa, O.: Processes and patterns of oceanic nutrient limitation, Nature Geoscience, 6, 701–710, https://doi.org/10.1038/ngeo1765, 2013.

Moore, J., Doney, S. C., Kleypas, J. A., Glover, D. M., and Fung, I. Y.: An intermediate complexity marine ecosystem model for the global domain, Deep Sea Research Part II: Topical Studies in Oceanography, 49, 403–462, https://doi.org/10.1016/S0967-0645(01)00108-4, 2001.

Shchepetkin, A. F. and McWilliams, J. C.: The regional oceanic modeling system (ROMS): a split-explicit, free-surface, topography-following-coordinate oceanic model, Ocean Modelling, 9, 347–404, https://doi.org/10.1016/j.ocemod.2004.08.002, 2005.

Stramma, L., Bange, H. W., Czeschel, R., Lorenzo, A., and Frank, M.: On the role of mesoscale eddies for the biological productivity and biogeochemistry in the eastern tropical Pacific Ocean off Peru, Biogeosciences, 10, 7293–7306, https://doi.org/10.5194/bg-10-7293-2013, 2013.

Thamdrup, B., Dalsgaard, T., Jensen, M. M., Ulloa, O., Farías, L., and Escribano, R.: Anaerobic ammonium oxidation in the oxygen-deficient waters off northern Chile, Limnology and Oceanography, 51, 2145–2156, https://doi.org/10.4319/lo.2006.51.5.2145, 2006.

Thomsen, S., Kanzow, T., Krahmann, G., Greatbatch, R. J., Dengler, M., and Lavik, G.: The formation of a subsurface anticyclonic eddy in the Peru- Chile Undercurrent and its impact on the near-coastal salinity, oxygen, and nutrient distributions, Journal of Geophysical Research: Oceans, 121, 476–501, https://doi.org/10.1002/2015JC010878, 2016.

Tracey, J. C., Babbin, A. R., Wallace, E., Sun, X., DuRussel, K. L., Frey, C., Martocello III, D. E., Tamasi, T., Oleynik, S., and Ward, B. B.: All about nitrite: exploring nitrite sources and sinks in the eastern tropical North Pacific oxygen minimum zone, Biogeosciences, 20, 2499–2523, https://doi.org/10.5194/bg-20-2499-2023, 2023.

Wang, W.-L., Moore, J. K., Martiny, A. C., and Primeau, F. W.: Convergent estimates of marine nitrogen fixation, Nature, 566, 205–211, https://doi.org/10.1038/s41586-019-0911-2, 2019.

Yang, S., Gruber, N., Long, M. C., and Vogt, M.: ENSO-Driven Variability of Denitrification and Suboxia in the Eastern Tropical Pacific Ocean, Global Biogeochemical Cycles, 31, 1470–1487, https://doi.org/10.1002/2016GB005596, 2017.

Zakem, E. J., Mahadevan, A., Lauderdale, J. M., and Follows, M. J.: Stable aerobic and anaerobic coexistence in anoxic marine zones, The ISME Journal, 14, 288–301, https://doi.org/10.1038/s41396-019-0523-8, 2020.